The 2140 cm^{-1} (4.673 μm) Solid CO Band: The Case for Interstellar O_2 and N_2 and the Photochemistry of Non-Polar Interstellar Ice Analogs

Jamie Elsila[1], Louis J. Allamandola[2], and Scott A. Sandford

NASA-Ames Research Center, MS 245-6

Moffett Field, CA 94035

Submitted to : *The Astrophysical Journal*, June 3, 1996

Suggested Running Title: Interstellar CO, N_2, O_2, and CO_2 Ices

Keywords: interstellar CO

interstellar N_2

interstellar O_2

interstellar chemistry

interstellar ices

cometary ices

spectroscopy, infrared

photochemistry

1.- Current Address: 1411 Three Mile, Grosse Pointe Park, MI, 48230

2 - Author to whom correspondence should be addressed.

ABSTRACT

The infrared spectra of CO frozen in non-polar ices containing N_2, CO_2, O_2, and H_2O, and the UV photochemistry of these interstellar/precometary ice analogs are reported. The spectra are used to test the hypothesis that the narrow 2140 cm^{-1} (4.673 μm) interstellar absorption feature attributed to solid CO might be produced by CO frozen in ices containing non-polar species such as N_2 and O_2. It is shown that mixed molecular ices containing CO, N_2, O_2, and CO_2 provide a very good match to the interstellar band at all temperatures between 12 and 30 K both before and after photolysis. The optical constants (real and imaginary parts of the index of refraction) in the region of the solid CO feature are reported for several of these ices.

The best matches between the narrow interstellar band and the feature in the laboratory spectra of non-polar ices are for samples which contain comparable amounts of N_2, O_2, CO_2, and CO. Coadding the CO band from an N_2:O_2:CO_2:CO = 1:5:$^1/_2$:1 ice with that of an H_2O:CO = 20:1 ice provides an excellent fit across the *entire* interstellar CO feature. The four component, non-polar ice accounts for the narrow 2140 cm^{-1} portion of the feature which is associated with quiescent regions of dense molecular clouds. Using this mixture, and applying the most recent cosmic abundance values, we derive that between 15-70% of the available interstellar N is in the form of frozen N_2 along several lines of sight towards background stars. This is reduced to a range of 1-30% for embedded objects with lines of sight more dominated by warmer grains. The cosmic abundance of O tied up in frozen O_2 lies in the 10-45% range toward background sources, and it is between 1 and 20% towards embedded objects. The amount of oxygen tied up in frozen CO and CO_2 can be as much as 2-10% toward background sources and on the order of 0.2-5% for embedded objects. Similarly, 3 to 13% of the carbon is tied up in frozen CO and CO_2 toward field stars, and 0.2 to 6% toward embedded objects. These numbers imply that most of the N is in N_2, and a significant fraction of the available O is in O_2 in the most quiescent regions of dense clouds.

As is well known, very weak infrared activity of the N_2 and O_2 stretching fundamental is induced in these types of ices. N_2 produces an absorption feature at 2328 cm^{-1} (4.296 μm) and O_2 produces an absorption feature near 1549 cm^{-1} (6.456 μm).

Ultraviolet photolysis of these ices produces a variety of photoproducts including CO_2, N_2O, O_3, CO_3, HCO, H_2CO, and possibly NO and NO_2. XCN is not produced in these experiments, placing important constraints on the origin of the enigmatic interstellar XCN feature. N_2O and CO_3 have not been previously considered as interstellar ice components, but can be searched for using their strongest fundamental bands which fall near 2235 and 2041 cm^{-1} (4.474 and 4.900 μm) respectively. These bands fall at frequencies that are inaccessible to ground-based observatories but which are currently being explored by the ISO satellite.

1. INTRODUCTION

CO is the most abundant diatomic interstellar molecule after H_2. Following its discovery in the interstellar gas by Wilson, Jefferts, and Penzias in 1971, CO quickly became the most studied of gas phase interstellar molecules. Indeed, it has proven to be a very powerful diagnostic of conditions in a wide variety of astronomical environments and has given great insight into structure on a galactic scale (Latter et al. 1996). Although the possibility that CO might also be frozen on interstellar grains and in comets had been postulated for some time (c.f. Herzberg 1955; Ewing, Thompson, & Pimentel 1960), the serious study of interstellar *solid* state CO had a slow start.

The discovery of infrared absorption in the vicinity of the feature now attributed to CO frozen on grains was made by Soifer et al. (1979) in the spectrum of the embedded protostar W33A. Due to insufficient resolution, and the fact (then unknown) that this region of the spectrum of W33A is dominated by the XCN band centered at 2165 cm^{-1} (4.619 μm), the authors reasoned that the absorption probably arose from CO, either in the gas or solid state, but they could not account for the apparent peak shift with respect to the expected position of about 2140 cm^{-1} (4.673 μm). The first comparison between this spectrum (and the spectra of other embedded objects) with the spectrum of an interstellar ice analog containing CO was made by Hagen, Allamandola, and Greenberg (1980). In discussing the interstellar spectra, they pointed out that, "The very important null gap (missing Q branch) region between 2135 and 2140 cm^{-1} is not yet available at very high resolution. It is difficult to overemphasize the importance of this region because the mid-infrared

spectrum of a heterodiatomic molecule such as CO is very different depending on whether or not the molecule is in the gas or solid phase." This ultimately led to the first high resolution observations of W33A in this spectral region and the clear-cut detection of CO frozen on interstellar grains by Lacy et al. (1984). The observations showed that the low resolution feature in W33A detected by Soifer et al. consisted of three bands: a strong, very broad absorption at 2165 cm^{-1} (4.619 μm, FWHM = 28 cm^{-1}), a weak, narrow band at 2140 cm^{-1} (4.673 μm, FWHM = 5 cm^{-1}), and an even weaker, broad feature at 2135 cm^{-1} (4.684 μm, FWHM = 12 cm^{-1}). [These FWHM are the full width at half maximum of the bands when plotted in absorbance, or optical depth.] Based on comparisons with the spectra of laboratory analogs, Lacy et al. showed that the 2135 and 2140 cm^{-1} bands arise from solid CO, and that the 2165 cm^{-1} band was due to the CN stretch in an unidentified species designated XCN.

Following this work, the study of solid state interstellar CO began in earnest. Over the next few years the CO feature was detected along several lines of sight through the Taurus dark cloud (Whittet, Longmore, & McFadzean 1985; Whittet et al. 1989) and toward a number of protostellar objects embedded in dense clouds (Geballe 1986). Taken together, these observations showed that: (i) the 2135 and 2140 cm^{-1} bands were both evident in the spectra of many clouds, (ii) the amount of solid CO varied with respect to other interstellar ice components such as H_2O, and (iii) the spectra of some embedded objects did not show any solid state CO absorption.

During this same period, laboratory spectral analysis of CO-containing ices (Sandford et al. 1988) led to the following conclusions: (i) the broad 2135 cm^{-1} band is most likely due to CO frozen in an H_2O-rich ice with an H_2O:CO ratio greater than 5, (ii) the narrower 2140 cm^{-1} band could not be due to CO intimately mixed with H_2O or any other polar ice species likely to be important in molecular clouds, and (iii) the narrower band could be matched by CO frozen in certain non-polar ices. Of the ices studied by Sandford et al., those dominated by CO_2 provided the best fits to the interstellar 2140 cm^{-1} feature. That some of the interstellar CO was frozen in a non-polar ice came as something of a surprise since the 3250 cm^{-1} (3.08 μm) H_2O ice feature dominated the infrared spectra of dense clouds, leading to the belief that H_2O was the major component of interstellar ices.

By 1989, however, evidence was starting to mount that more CO was frozen in non-polar ices than in polar, H_2O rich ices. The 2140 cm^{-1} CO band toward SVS 20 (CK 20) in the Serpens molecular cloud measured by Eiroa and Hodapp (1989) was much stronger than the broader 2135 cm^{-1} feature corresponding to CO frozen in H_2O. Band depth analysis implied an H_2O/CO column density ratio of 2.86, making CO the second most abundant mantle material along this line of sight. This was also the first case in which the peak optical depth of the 2140 cm^{-1} CO band exceeded the depth of the very strong 3250 cm^{-1} H_2O ice feature. Very thorough subsequent observations and analysis of the frozen CO feature along many lines of sight by Tielens et al. (1991) and Chiar et al. (1994, 1995) now make it clear that the 2140 cm^{-1} band is dominant along most lines of sight through quiescent regions of dense clouds. Based on the laboratory data of Sandford et al. (1988), Chiar et al. (1994, 1995) showed that a significant fraction (~40 %) of the *total* CO abundance is found frozen in the non-polar ices, with the solid CO column density typically being ~30% that of H_2O along these same lines of sight. In contrast, no more than a few percent of the available CO is frozen onto the grains along the lines of sight toward embedded protostars such as W33A (6%; Mitchell, Allen, & Maillard 1988, Mitchell et al. 1990) where most of the frozen CO is in the polar, H_2O-rich ices that produce the 2135 cm^{-1} band.

Recent reviews of these observations in the context of a general overview of interstellar molecular ices have been given by Whittet (1993) and Sandford (1996a,b). Other laboratory studies which provide data that is of relevance for interstellar CO ice include a study of the binding energies and vaporization properties of frozen CO (Sandford & Allamandola 1990a), the temperature behavior of the 2135 cm^{-1} band due to CO in H_2O ice (Schmitt, Greenberg, & Grim 1989), the behavior of the infrared band for frozen CO as a function of ion irradiation and temperature (Palumbo & Strazzulla 1993), the optical constants for CO frozen in a number of mixtures (Hudgins et al. 1993, 1994), and band strengths refined to an accuracy of a few percent for the solid CO band of pure CO and CO frozen in a number of mixtures (Gerakines et al. 1995).

Despite the great amount of lab work and the ever increasing number of astronomical spectra, the exact identity of the solid ice matrix that produces the narrow CO absorption at 2140 cm^{-1} has

remained uncertain. Sandford et al.(1988) showed that, of the non-polar ice constituents considered in their extensive laboratory study, CO frozen in a CO_2-rich ice came closest to matching the interstellar band position. Using this laboratory data, Eiroa and Hodapp (1989), Tielens et al. (1991), Kerr, Adamson, and Whittet (1991), and Chiar et al. (1994, 1995) have shown that most of the interstellar features could be matched by coadding the profiles of CO_2:CO, H_2O:CO, and O_2:CO ices, with the best fits requiring coadding different amounts of ices with differing ratios for different objects.

While the matches to the 2140 cm^{-1} band are reasonably good, they are not perfect and several doubts remain. For example, invoking varying amounts of three different binary ices seems somewhat contrived. Furthermore, the laboratory spectra do not reproduce the interstellar band profile in detail, especially on the high-frequency side. In addition, comparisons of laboratory spectra of CO in CO_2 with astronomical observations are satisfactory only over a limited temperature range (Tielens et al. 1991) and at high concentrations of CO_2 (CO_2/CO = 20). It is difficult to understand how so much CO_2 could be present. Models of interstellar chemistry cannot account for the large amount needed (Tielens & Hagen 1982; d'Hendecourt, Allamandola, & Greenberg 1985). The limited observations which are available for CO_2 also suggest that the abundance of frozen CO_2 is roughly equal to that of solid CO along those lines of sight which have some contribution from quiescent regions (d'Hendecourt and Jourdain de Muizon 1989). Orbital infrared telescopes equipped with spectrometers capable of resolving the CO_2 bands such as the recently launched Infrared Space Observatory (ISO) will certainly place important further constraints on the amount of CO_2 frozen on interstellar grains.

Since there are some doubts regarding CO_2-rich ices, other suggestions for possible origins of this feature have been considered. These include pure frozen CO, and CO-rich ices containing H_2O at a H_2O/CO ratio of about $^1/_{10}$ (Tielens et al. 1991), and ion irradiated pure CO and mixed molecular ices (Palumbo & Strazzulla 1993). While the suggestion of pure CO ices seems unlikely due to the amount of other species available in the interstellar medium, CO-rich mixtures, ion irradiated or not, are plausible. Indeed, our studies of UV irradiated H_2O-rich mixed molecular ices

also shift the frozen CO feature into close agreement to the 2140 cm^{-1} position. However, these radiation processes should be less important in the quiescent regions of clouds characterized by the 2140 cm^{-1} band than toward protostellar regions where the 2135 cm^{-1} band is more important.

In view of these questions, we have studied the CO band in ices containing various mixtures of CO, N_2, O_2, CO_2, and H_2O in an attempt to understand the origin of the narrow 2140 cm^{-1} interstellar absorption band. The three non-polar species N_2, O_2, and CO_2 have been chosen because theoretical models of interstellar ice grain chemistry have long predicted that these species are important in certain dense cloud environments (Tielens & Hagen 1982; d'Hendecourt et al. 1985). We have also investigated the photolysis of these ices, as photochemical studies of non-polar interstellar ice analogs are quite scarce.

In the following section (§2), we briefly discuss the experimental techniques used in this study. The spectroscopic data and photochemical results are presented in §3 along with the optical constants (real and imaginary parts of the index of refraction - n's and k's) across the solid CO band for several relevant interstellar ice analogs. In §4 we compare these results to astronomical data and conclude that interstellar ices made up of N_2, O_2, and CO_2 are plausible. The astrophysical implications of these results are discussed in §5, including the implied N_2 and O_2 interstellar abundances and depletions, and the new interstellar grain species suggested by the photolysis experiments. The main conclusions are summarized in §6.

2. EXPERIMENTAL METHODS

Only a brief summary will be given here, since the general procedures used have been described elsewhere (Allamandola, Sandford, & Valero, 1988; Sandford et al. 1988), . Glass bulbs containing the gas mixtures to be studied were prepared in a greaseless, glass vacuum system. Gas samples (CO, Matheson C.P., 99.5% purity; CO_2, Matheson Bone Dry, 99.8% purity; O_2, Matheson Extra Dry, 99.6% purity) were introduced into the glass vacuum line directly from lecture bottles without further purification. N_2 (Airco Dry, 99.9% purity) was introduced into the sample preparation line only after passage through a liquid nitrogen cooled trap. H_2O

(triply distilled) was further purified by three freeze-pump-thaw cycles before use. Once prepared, each mixture was allowed to equilibrate overnight.

After transferring the bulb to the cryogenic sample preparation system, the mixture was then deposited under vacuum onto a cold (~12 K) CsI substrate. The deposition rate was typically between 10^{-2} and 10^{-1} moles/hr. Deposition times for these experiments ranged from 2 seconds to 30 minutes. The infrared spectrum of the resulting amorphous ice was then recorded using a Fourier transform infrared spectrometer. All spectra are presented here in percent transmittance and the FWHM listed in the Tables correspond to percent transmittance, not optical depth or absorbance. Subsequently, the ice was warmed in steps to higher temperatures, and the infrared spectrum recorded at each temperature.

Ultraviolet photolysis of several mixtures was carried out using a microwave-powered hydrogen flow lamp. An H_2:He = 1:9 gas mixture was used in the photolysis lamp. This enhances the 1216 Å Lyman α line emission relative to general continuum emission. The ices were kept at 12 K during the irradiation periods, which were typically about three hours. In cases where the samples were photolyzed, the spectrum was recorded before and after irradiation as well as during warm-up.

3. EXPERIMENTAL RESULTS

Table 1 presents a summary of all the mixtures examined as part of this study. Entries in parentheses indicate the mixtures which were photolyzed. The results are presented as follows. First, the frozen CO band profile dependence on concentration in binary N_2:CO mixtures is described in §3.1.1. Second, the influence of H_2O on the CO peak position and profile in N_2:H_2O:CO ices is discussed in §3.1.2. Third, the effects of the presence of other molecules such as CO_2 and O_2 on the solid CO feature with and without N_2 are considered in §3.1.3. Lastly, four component ices comprised of N_2:O_2:CO_2:CO are described in §3.1.4. In all cases, the CO band temperature dependence was also studied. The photochemistry of a few of the ices is described in §3.2., and the optical constants of a number of the ice mixtures studied here are presented in §3.3. Finally, the bands produced by solid N_2 and O_2 are discussed briefly in §3.4.

All measurements of peak positions and widths presented in the Tables were made from the original spectra. However, the baselines were flattened for the Figures in those cases where the spectra showed significant tilts or curvature, or contained strong interference fringes. All spectra are presented in percent transmittance and the FWHM listed in the Tables correspond to percent transmittance plots, not optical depth or absorbance. The data are plotted in this way since this permits a better assessment of the fit across the entire feature.

3.1. *The Frozen CO Feature in Non-Polar Ices*

3.1.1. *N_2:CO Ices*

A series of mixed-molecular ices having different N_2:CO concentrations were studied. The N_2 to CO ratios were chosen to bracket plausible interstellar ratios associated with a range of possible environments. The spectra of these ices were measured at 12 K and at several temperatures up to 35 K. The profiles of the CO bands are shown in Figure 1 and peak positions and widths are listed in Table 2. Values are only given in the table at those temperatures where a measurable, reproducible change occurred in position or width during warm up. Figure 2 shows the change in the CO profile that occurs upon warm-up of the N_2:CO = 1:20 ice. Solid nitrogen starts to sublime between 30 and 35 K under these high-vacuum conditions. The sudden shift in position, increase in width, and decrease in strength above ~ 30 K listed in Table 2 for the N_2:CO = 25:1 and 2:1 ices corresponds to the temperatures at which the nitrogen softens and begins to sublime, releasing much of the trapped CO. The profile of the CO band is broader because it is in a much less rigid, more irregular cage.

3.1.2. *N_2:H_2O:CO Ices*

Since H_2O is an abundant interstellar ice constituent, a series of ices containing N_2, CO, and H_2O were also prepared and studied. The relative amounts of each component were varied in order to be able to bracket a wide range of H_2O concentrations in the ices. Ices dominated by H_2O were not considered here since they have been discussed elsewhere (cf. Sandford et al. 1988). The CO bands produced by these ices are shown in Figure 3, with band positions and FWHM

listed in Table 3. In many of these ices a second band appeared near 2148 cm^{-1} (see also Sandford et al. 1988; Schmitt et al. 1989; Palumbo & Strazzulla 1993). This feature has been attributed to a second CO trapping site in amorphous H_2O ices (Sandford et al. 1988). These data suggest that the second site is characterized by a dangling OH bond which forms a weak complex with the CO. Positions and widths for this second band are listed in parenthesis in Table 3. Sandford et al. (1988) and Schmitt, Greenberg, and Grim (1989) have studied the temperature behavior of the 2148 and 2135 cm^{-1} bands.

3.1.3. *O_2:CO, CO_2:CO, N_2:O_2:CO, and N_2:CO_2:CO Ices*

As the 2140 cm^{-1} feature is indicative of CO in a non-polar ice, binary mixtures of CO in O_2 and CO_2 were studied to compare with the N_2-containing ices since these species are also likely to be abundant in quiescent regions of dense molecular clouds (Tielens & Hagen 1982; d'Hendecourt et al. 1985). Several trinary mixtures containing CO with N_2 and O_2, or N_2 and CO_2 were also investigated. The results of these experiments are listed in Table 4 and shown in Figures 4 and 5.

3.1.4. *N_2:O_2:CO_2:CO Ices*

Comparison of the spectra presented in §3.1.1. to §3.1.3. with interstellar spectra shows that combinations of binary and trinary ices containing CO with N_2, O_2, and CO_2 are required to produce a band consistent with the interstellar feature. Consequently, a few four component ices containing N_2, O_2, CO_2, and CO were also studied. The results of these experiments are listed in Table 4 and shown in Figure 6.

3.2. *Photochemistry*

The UV photochemistry of the seven ice mixtures listed in parentheses in Table 1 was also studied. The infrared spectra of the mixtures taken after UV photolysis were compared with preirradiation spectra to identify photoproducts and to monitor the effect of photolysis on the solid CO feature. As an example, the 2000 to 500 cm^{-1} (5 to 20 μm) spectrum of the N_2:O_2:CO = 1:1:1 ice is shown both before and after photolysis in Figure 7. Photolysis for periods longer than three

hours did not produce further significant spectral changes. Four types of ices were irradiated: N_2:CO mixtures, N_2:H_2O:CO mixtures, an N_2:O_2:CO mixture, and an N_2:O_2:CO_2:CO mixture. The photoproducts and their relative abundances varied, depending on the initial ice composition. The bands due to the photoproducts from two different ices are shown in Figures 8 and 9. Identifications of the new features appearing upon photolysis are listed in Table 5. Table 6 compares the peak positions and FWHM of the CO feature before and after photolysis for all seven mixtures.

Most of the photochemistry is driven by reactions with "hot" O atoms liberated by photolysis of O_2, H_2O, or CO (Figures 8 and 9). The principle species produced from O atom reactions are CO_2, N_2O, O_3, and CO_3. CO_2 is detected in all cases, and N_2O in most. As the concentration of CO decreases (especially in the N_2:CO series of ices), N_2O production is favored over CO_2 production. Conversely, an increase in CO concentration in the N_2:CO series of experiments does not favor the appearance of any other new photoproducts except CO_2. Ozone appears as a photoproduct in all the mixtures, although the amount produced is highly variable. Relatively little O_3 is produced in the N_2:CO and N_2:H_2O:CO ices, probably due to the lower availability of photolytic oxygen atoms present in the starting mixtures. The N_2:O_2:CO and N_2:O_2:CO_2:CO ices show the strongest ozone production as measured by the strength of the 1037 cm^{-1} (9.643 μm) ozone band. Here, enough ozone is produced that even the weaker 2108, 1104, and 704 cm^{-1} (4.744, 9.058, and 14.20 μm) O_3 bands are evident. Again, this result is expected as copious "hot" O atoms are produced by the photolysis of O_2 under these conditions. The "hot" O atoms readily combine with undissociated O_2 molecules to produce O_3. Photolysis of the molecular oxygen-containing ices also produced carbon trioxide (CO_3), presumably by the addition of O to CO_2.

The liberation of hydrogen in the H_2O-containing mixtures produces the formyl radical (HCO), which appeared in low concentration in both H_2O mixtures, and formaldehyde (H_2CO), which was detected only in the more H-rich N_2:CO:H_2O = 2:1:1 ice. Since formaldehyde requires the addition of one more hydrogen atom than the formyl radical, it is not surprising that it appears only when the H_2O concentration is high. Several other very weak features appeared between

1900 and 1750 cm^{-1} (5.26 and 5.71 μm) in the H_2O containing ices. These presumably arise from various hydrogenated forms of CO and CO_2 such as HOCO (Milligan & Jacox 1971).

There is some evidence for the production on NO_2 and NO, but it is inconclusive. NO_2 absorbs at 1610 cm^{-1} in an argon matrix, at 1612 cm^{-1} in an O_2 matrix (St. Louis & Crawford 1965), and at 1617 cm^{-1} in a N_2 matrix (Lucas & Pimentel 1979). Thus, the band which appears near 1607 cm^{-1} after photolysis of several ices may arise from NO_2, but one would expect it to fall closer to the 1612 or 1617 cm^{-1} positions since the mixed molecular ice environment is closer to that of solid O_2 or N_2 rather than solid Ar. Similarly, NO absorbs at 1875 cm^{-1} in Ar and at 1883 cm^{-1} in CO_2 matrices, respectively (Fateley, Bent, & Crawford 1959). Sharp, very, very weak absorptions appear at 1875 and 1860 cm^{-1} upon photolysis of the N_2:CO = 100:1 and 2:1 ices, respectively, and a sharp, weak absorption appears near 1860 cm^{-1} in the N_2:H_2O:CO = 2:1:1 ice. Again, the new band falls more than 20 cm^{-1} lower than the position expected based on the published matrix isolation studies. Furthermore, if the 1607 cm^{-1} band is due to NO and the 1875 or 1860 cm^{-1} absorptions are due to NO_2, some correlation between these two features would be expected. However, none is seen in this limited set of data. Thus, while the spectra are suggestive of NO_2 and NO production, doubts remain.

3.3. *Optical Constants (n +ik)*

The real and imaginary parts of the indices of refraction (n and k) were determined for a number of the ices studied using a Kramers-Kronig analysis (Bergmen et al. 1978) of the transmission spectra. The procedure was essentially that used by Hudgins et al. (1993) to determine the optical constants of a wide variety of mixed molecular ices of astrophysical interest (see also Hudgins et al. 1994). Readers interested in the details of the calculation of the optical constants should see Hudgins et al. (1993).

Briefly, the computational procedure used to determine the complex index of refraction was as follows. Assuming a starting value for $\boldsymbol{n}$ [= $n_0 = n_{(\mathrm{Na\ D})}$] at all frequencies, a Kramers-Kronig analysis was used to calculate the absorption coefficient and the imaginary part of the refractive index across the spectral region of interest. The real part of the refractive index was then

computed. The resultant n and k values were used to compute a synthetic spectrum which was, in turn, compared to the real spectrum. Differences between the real and computed spectrum were then used to adjust the previously assumed $\boldsymbol{n}$ values. This iterative process was repeated, using the new $\boldsymbol{n}$ values generated from the previous step, until the calculated transmission spectrum differed nowhere from the measured value by more than 0.1% . The number of iterations required to fulfill this requirement depended on the number, strength, and width of the absorption features within the spectrum. For the spectra discussed here, the number of iterations required typically fell between 10 and 30, although spectra dominated by strong, narrow bands like those produced by CO_2 occasionally required almost 100. The correct operation of the program was initially verified by comparing our results against values already reported in the literature. Our technique gives good agreement with those reported for H_2O (Bertie et al. 1969; Hagen, Tielens, & Greenberg 1981; Leger et al. 1983), CO_2 (Wood & Roux 1982; Warren 1986), CO (Roux et al. 1980), and CH_4 (Roux et al. 1980; Pearl et al. 1991).

For ices dominated by N_2 and O_2, where CO produced the only absorption band of any significance, calculations were carried out only over the 2250-2050 cm^{-1} (4.44-4.88 μm) region using all the data points in the experimental spectrum in this interval (corresponding to ~1 point every 0.5 cm^{-1}). Ices containing CO_2 and H_2O, however, produce additional absorption features that must be accounted for. In these cases, the calculations were first made over the entire 4000-500 cm^{-1} (2.5 - 20 μm) region using every fifth data point in the experimental spectrum (corresponding to ~1 point every 2.5 cm^{-1}). The results of these calculations were then used to select appropriate n_o values for all data calculations from the same experimental spectra over the 2250-2050 cm^{-1} region. The results of the higher resolution calculations were then adjusted to fit the continuous portions of the lower resolution results.

The absolute accuracy of the resulting optical constants is limited mainly by uncertainty in the assumed starting value of the visible refractive index (n_o) of the ice sample and uncertainty in the measured sample thickness h. We have based our assumed n_o values on reported values for the visible refractive index of similar sample ices at the D lines of atomic Na (λ = 589 nm). For ices

dominated by CO_2, N_2, and O_2 we have used values of n_o = 1.22, 1.22, and 1.25, respectively (Hallam & Scrimshaw 1973). We used a value of n_o = 1.32 for H_2O-rich ices (Hudgins et al. 1993) and n_o = 1.30 for ices dominated by CO (Jiang et al. 1975). In the cases of ices that were not clearly dominated by a single component, the concentration weighted values of the different ice components were used to estimate a value. Uncertainty in the adopted values for n_o is due to the effect of the residual dispersion of the ultraviolet contributions to n_o between the visible and 4000 cm^{-1} and the dependence of n_o on the temperature, composition, and crystal structure of the sample. The effect of the above errors would largely be to impose a small global vertical shift on the resultant n values. Given the limited range of n_o values of these ices, we expect that the uncertainties associated with the values we have chosen are less than 5%.

The biggest difference between the techniques used by Hudgins et al. and those used here is that a laser was not used to determine sample thickness in this study. Here sample thicknesses were determined using two different methods. In many cases the samples were thick enough that a measurable portion of the infrared light underwent multiple reflections within the sample. This resulted in a sinusoidal interference pattern being superimposed on the overall spectrum. In these cases the thickness of the ice could be determined from the equation

$$d = \frac{N_{osc}}{2n\,(\nu_o - \nu_1)} \qquad (1)$$

where ν_o and ν_1 are the limits (in cm^{-1}) over which the oscillations due to interference are measured, N_{osc} is the number of fringes or 'wavelengths' of the oscillation occurring between ν_o and ν_1, and n is the index of refraction of the sample. In these cases, the accuracy of the thickness determination is largely limited by uncertainties in the value of n , uncertainties are probably less than 5%.

Absorption band strengths were used to estimate sample thicknesses in those cases for which the ice samples were too thin to produce measurable interference fringes. In this situation, the column density, N (in molecules cm^{-2}), of different molecular species within the sample was determined using the equation

$$N_i = \frac{\int \tau_i(\nu)\, d\nu}{A_i} \qquad (2)$$

where $\tau_i(\nu)$ is the frequency-dependent optical depth (in absorbance) of an absorption band and A_i is the band's integrated absorbance (in cm molecule^{-1}) as determined from laboratory studies (cf. d'Hendecourt & Allamandola 1986; Hudgins et al. 1993). Column densities determined in this manner could be used with the known concentrations of the different molecules in the sample and a sample density based on matrix site sizes (Hallam & Scrimshaw 1973) to estimate a sample thickness. This technique is inherently less accurate that the interference technique because the actual densities and A_i values for these mixed molecular ices have not been measured and they can only be estimated from values obtained from similar, but less complex ices. When this technique was used on ice samples for which we had independent thickness determinations from interference measurements, it was found that thicknesses based on absorption band strengths fell within 50% of the values determined from fringe analysis.

A summary of the n and k values of the CO feature in a number of ices are listed in Table 7. The values we assumed for $n_{(NaD)}$ and d for each sample are also in the Table. It can be seen that the majority of our sample thicknesses fell within the 0.1 - 5.0 μm range, although ices dominated by strong absorbers like CO_2 were occasionally thinner and ices dominated by weak absorbers such as N_2 and O_2 were occasionally thicker. The expected absolute accuracies of these values differ from ice to ice and depend largely on uncertainties in the sample thicknesses. For ices whose thicknesses were determined from interference fringes produced by internal reflections (N_2:CO=2:1, O_2:CO=20:1, N_2:H_2O:CO=2:1:1), we estimate the *absolute* uncertainty of the calculated optical constants to be about 5%. Uncertainties differ for ices where the thickness could only be estimated from absorption band strengths. For the pure CO ice and the ices H_2O:CO=20:1 and CO_2:CO=20:1, where A values have been measured for similar ices, absolute uncertainties are probably less than 10%. The uncertainties associated with the other ices listed in Table 7

(N_2:O_2:CO_2:CO=1:5:$^1/_2$:1, N_2:CO_2:CO=1:5:1, N_2:H_2O:CO =5:1:5, N_2:O_2:CO=1:5:1) are likely to be similar, but could be as large as 50%. We stress, however, that the *relative* errors between adjacent n and k pairs in all the columns are less than 0.1%, the limiting difference between the measured and calculated spectra at which we chose to terminate our iterative calculations.

3.4. *The Fundamental Bands of Solid N_2 and O_2*

Although neither N_2 nor O_2 have allowed infrared transitions, it has long been known that infrared activity is induced when these species are condensed (Smith, Keller, & Johnston 1950). Use of this effect has been proposed by Ehrenfreund et al. (1992) to search for frozen, interstellar O_2, and was exploited by Sandford, Allamandola, & Geballe (1993) to detect frozen interstellar H_2.

The N_2 band falls at 2327.7 cm^{-1} (4.2961 μm) (Figure 10) in a spectral region obscured by telluric CO_2. The 2327.7 cm^{-1} band has been well studied and is readily attributable to N_2 (Moll, Clutter, & Thompson 1960; Lowen, Bier, & Jodl 1990; Grundy, Schmitt, & Quirico 1993; Bohn et al. 1994; Tryka, Brown, & Anicich 1995). The assignment of the feature at 2347.4 cm^{-1} (4.260 μm) has been more problematic. This position is characteristic of the asymmetric stretching vibration of CO_2 in N_2, but previous investigators of the spectrum of N_2 ices who have noted this feature have been unwilling to unequivocally assign it to contaminant CO_2 (Tryka et al. 1995). Indeed, many of our own spectra that contain this feature fail to show the characteristic O=C=O bend mode band of CO_2 near 660 cm^{-1}. However, recent unpublished data taken in our laboratory have demonstrated that the well known 2327.7 cm^{-1} N_2 band shifts to lower frequencies when $^{15}N_2$ is used, but the 2347.4 cm^{-1} feature does not. Thus, we feel the 2347.4 cm^{-1} feature is due to extremely small amounts of contaminant CO_2.

As discussed by Ehrenfreund et al. (1992), O_2 frozen in mixed-molecular ices also has weak infrared activity. Figure 11 shows the O_2 band in a N_2:O_2:CO = 1:1:1 ice before and after three hours of UV irradiation. The feature falls near 1549 cm^{-1} (6.456 μm).

4. THE INTERSTELLAR CO BAND AND NON-POLAR ICES

The previous results will now be discussed in an astrophysical context. The spectra in Tielens et al. (1991) and Chiar et al. (1994, 1995) show that the 2140 cm^{-1} component usually dominates the interstellar absorption feature associated with frozen CO along most lines of sight. In addition to this feature, all lines of sight also have some contribution from the 2135 cm^{-1} band which is associated with CO in H_2O-rich ices. In the following sections we compare the interstellar CO feature, especially the 2140 cm^{-1} component, with those of the laboratory analogs described above and use these comparisons to place constraints on the interstellar ice composition. Figures 12 and 13 show interstellar CO bands representative of the features that must be matched. The astronomical spectra in these figures are taken from Tielens et al. (1991). Comparisons between the astronomical and laboratory spectra are make in transmittance, not optical depth units as is customery, in order to facilitate comparison across the entire feature.

4.1. *N_2:CO Ices*

The data in Table 2 and Figure 1 show that the position and width of the CO feature depends upon the ratio of N_2 to CO in these ices. Comparison of the N_2:CO ice spectra with the interstellar CO features given in Figures 12 and 13 show that while the more dilute mixtures (N_2:CO = 25:1 and 100:1) match the position of the interstellar peak reasonably well, they are far too narrow (1.0-1.3 cm^{-1} versus a more typical width of ~10 cm^{-1} for the interstellar band). In the N_2:CO = 2:1 and 1:20 ices, the peak frequency is too low by about 1 cm^{-1} and the width is still too narrow (between 2-3 cm^{-1}). This trend is consistent with the 0.18-0.013 cm^{-1} linewidths reported by Dubost, Charneau, and Harig (1982) for CO in N_2 matrices at mole fractions of 10^{-2} to 10^{-5}, respectively. The mismatches in position and width are not improved by warming (Figure 2, Table 2) or photolysis (Table 6). These experiments also demonstrate that in order for interstellar (and cometary) ices to contain appreciable amounts of N_2, they must remain well below 30 K (see Figure 2).

In summary, while the band positions are consistent with the hypothesis that CO can be frozen along with N_2 in these interstellar clouds, this series shows that ices made solely of CO and N_2 do not fit the interstellar feature in a satisfactory manner because they produce bands that are too narrow.

4.2. *N_2:H_2O:CO Ices*

The addition of a third plausible component to the N_2:CO mixtures improves the situation somewhat. Given that H_2O is the most abundant molecule frozen on interstellar grains, it is a logical third component to consider. The spectral properties of the CO band produced by N_2:H_2O:CO ices are shown in Figure 3 and summarized in Table 3. The CO peak frequencies of these ices span the range from 2139.7 to 2139.1 cm^{-1} and consistently match the interstellar peak position better than those of the binary N_2:CO mixtures. In addition, the bands are broader and their widths best match that of the interstellar feature when the concentrations of N_2, H_2O, and CO are comparable. Of the mixtures we have studied, the N_2:H_2O:CO = 2:1:1 ice, having a peak position of 2139.2 cm^{-1} and a FWHM of 5.3 cm^{-1}, produces a CO feature which comes the closest of these ices to matching the interstellar band. The data listed in Tables 3 and 6 show that the CO feature in these trinary mixtures is not altered much by photolysis or warming over the entire range of temperatures at which the N_2 ice is stable.

However, a high-frequency feature near 2148 cm^{-1}, absent from the interstellar spectra, is also produced in many of the ices which contain H_2O. It is most intense when the H_2O concentration is high, and becomes almost unobservable at very low H_2O concentrations (Figure 3, Table 3). The ices which produce the best fits to the 2140 cm^{-1} interstellar feature have some of the strongest 2148 cm^{-1} bands. Since this second band always appears in the spectra of ices containing substantial amounts of H_2O, and it is not evident in the interstellar spectra (although telluric obscuration does not permit the full spectral coverage required to search unambiguously for the high frequency band), we rule out ices in which the H_2O concentration is comparable to, or greater than, that of the other non-polar components as carriers of the 2140 cm^{-1} band. Conversely, while lower H_2O concentrations such as that in the N_2:H_2O:CO = 5:1:5 ice do not show a 2148 cm^{-1} band (Figures 3 & 12) and produce a CO band which comes close to the interstellar peak

frequency, they are too narrow and fall ~1 cm^{-1} to the red of the interstellar position (see Figure 12). Thus, mixtures which contain *minor* amounts of polar molecules but which are dominated by non-polar species, could contribute to the interstellar feature, but cannot fully explain it.

A better understanding of the importance of H_2O in interstellar CO-containing ices can be obtained by spectral coverage of the entire 2180-2100 cm^{-1} (4.59-4.76 μm) region using spaceborne instrumentation, since such data would allow an unambiguous search for evidence of the 2148 cm^{-1} feature.

4.3. *O_2:CO, CO_2:CO, N_2:O_2:CO, and N_2:CO_2:CO Ices*

The data in Table 4 and Figures 4 and 5 show that simple binary mixtures of O_2:CO, and CO_2:CO cannot reproduce the peak position, FWHM, and profile of the interstellar feature. In the case of O_2:CO, the position is too low by about 3 cm^{-1} and the band too narrow by about 5 cm^{-1}. Although the CO_2:CO = 20:1 mixture has been used to fit the interstellar feature in the past, it too is inadequate since it has a high frequency wing not seen in the interstellar band profile.

While an O_2:CO = 20:1 mixture does not match the position or width of the interstellar feature, three component N_2:O_2:CO mixtures do a bit better. Both the N_2:O_2:CO = 1:1:1 and 1:5:1 mixtures have CO features which peak about 1 to 2 cm^{-1} to the red and are too narrow by several cm^{-1} (see Figure 12). Table 6 shows that photolysis does not alter the frequency to better match the interstellar band position, and although it increases the width of the CO feature in the N_2:O_2:CO = 1:1:1 ice from 4.0 cm^{-1} to 6.0 cm^{-1}, it is still too narrow.

A similar study of the influence of CO_2 on the CO band in N_2:CO ices leads to the following conclusions. In the lowest concentration case (N_2:CO_2:CO = 1:1:1), the CO band is blue shifted into closer agreement with the interstellar band by nearly 1 cm^{-1}, but it remains far too narrow. Higher concentrations of CO_2 produce even more widening and blue shifting of the band. The N_2:CO_2:CO = 1:5:1 ice has a CO feature that is blue shifted by 2 cm^{-1} to 2141.5 cm^{-1}, a frequency 1 cm^{-1} *too* high for the interstellar feature, and it is broadened to a FWHM of 9.6 cm^{-1} (see Figure 12). The CO_2, which is too large to fit into the N_2 lattice, presumably breaks up the regularity of

the N_2 matrix, causing the band to shift slightly to the blue and adding extra absorbance to the high frequency wing of the feature.

The principle conclusions from the best fits to the interstellar feature found in this and the previous two sections can be summarized by examining Figure 12. Three-component non-polar ices such as N_2:O_2:CO = 1:5:1, or non-polar ices with a low concentration of a polar species such as H_2O (N_2:H_2O:CO = 5:1:5), produce features which peak near 2139 cm^{-1}, approximately 1 cm^{-1} to the red of the interstellar peak position. In both cases, the bands are too narrow, do not reproduce the peak position, and fail to account for the absorption on the high frequency side of the interstellar band. Of all the possible components studied here, CO_2 is the *only* one which can shift the CO absorption to frequencies up to and *higher* than the interstellar band peak position. This behavior suggests that an improved fit to the interstellar feature might best be provided by adding some CO_2 to ices like N_2:O_2:CO = 1:5:1, or possibly N_2:H_2O:CO = 5:1:5. This possibility is discussed below.

4.4. *N_2:O_2:CO_2:CO Ices*

The spectra in Figure 6 and data in Table 4 show the CO feature in ices made up of N_2, O_2, CO_2, and CO. The results of these four component ice experiments show that the roles played by the individual components in simpler ices are maintained, i.e. the N_2 and O_2 in the ices result in CO absorption centered near 2139 cm^{-1}, while the presence of CO_2 produces absorption above 2140 cm^{-1}. The best match to the interstellar feature is provided by N_2:O_2:CO_2:CO = 1:5:$^1/_2$:1. Ices with higher CO_2 concentrations produce too large a blue shift and too much absorption on the high frequency side of the band.

Figure 13 compares the profile of the CO ice feature of several laboratory ices with the spectra along four lines of sight through interstellar clouds. We have followed the common practice of fitting the entire interstellar feature with the combined absorption resulting from two very different ice components. The first component, H_2O:CO = 20:1, is added to account for the lower frequency 2135 cm^{-1} band produced by CO frozen in highly polar matrices (Sandford et al. 1988). This is only a minor component along most lines of sight (Tielens et al. 1991; Chiar et al. 1994,

1995). The second, and dominant, component is that of CO in a non-polar ice and it is added to provide the deeper, narrower 2140 cm^{-1} feature. In Figure 13a, we show the best fit that can be obtained to the spectrum of NGC 7538 IRS9 using H_2O:CO = 20:1 as the polar component and CO_2:CO = 20:1 as the non-polar component. While these two components have been used to fit interstellar data in the past, it is clear that this can be improved upon. In Figures 13b and 13c we show comparisons to the spectra of NGC 7538 IRS 9, Elias 16, AFGL 961, and Elias 18 where the CO_2:CO = 20:1 non-polar component is replaced with that of the N_2:O_2:CO_2:CO = 1:5:$^1/_2$:1 ice (see Figure 6). The fits utilizing the four component ice are considerably better across the entire feature. On the basis of these greatly improved fits *we conclude that an interstellar ice composition which best reproduces the 2140 cm^{-1} CO band characteristic of the quiescent regions of dense molecular clouds is one in which O_2 is important (comparable to or a few times more abundant than CO), the N_2 concentration is comparable to that of the CO, and the CO_2 concentration is less than that of the CO.*

5. ASTROPHYSICAL IMPLICATIONS

The results and analysis of the experiments described above will now be used to draw conclusions regarding the composition of interstellar ices in quiescent regions of dense molecular clouds. As pointed out by Tielens et al. (1991) and Chiar et al. (1994, 1995), the solid CO spectral characteristics of the lines of sight which probe the quiescent portions of molecular clouds can be quite distinct from those closely associated with embedded protostars. For example, the 2140 cm^{-1} component of the CO feature which is associated with non-polar ices is dominant toward field stars behind the Taurus molecular cloud and many other embedded objects, whereas it is almost negligible compared to the 2135 cm^{-1} component associated with CO trapped in H_2O-rich ices toward the embedded protostellar object W33 A. This suggests that the 2135 cm^{-1} band, and other unique characteristics of the spectrum toward W33A such as the prominent XCN and CH_3OH bands, are to be associated more with the environment of the protostar than with the molecular cloud itself. Perhaps in those cases in which the 2135 cm^{-1} component is more

dominent, the lines of sight sample 'distilled' ices in higher density material surrounding the protostar, perhaps material in the disk. In general, lines of sight to background stars are typically somewhat narrower that those towards embedded objects and require smaller contributions from the polar component (Fig. 13), consistent with this possibility. However, even the spectra background sources, such as Elias 16 (Fig. 13b), requires some contribution from the 2135 cm^{-1} band of polar ies. This implies that H_2O-rich ices are present in the quiescent regions of the cloud as well, but they are less important.

This overall behavior is consistent with the picture that the ices in the protostellar environment probed have probably undergone substantially more radiative processing and are somewhat warmer (i.e., well above 30 K) than those ices along lines of sight which have more obscuration arising in quiescent regions. At these warmer temperatures, the non-polar ices discussed here cannot survive, whereas H_2O-rich mixtures can. Therefore, throughout the following discussion we assume that the CO profile contains contributions from both non-polar and H_2O-rich polar ices, with the non-polar component dominating in the quiescent regions. Furthermore, we do not take Doppler shifts or scattering and grain size distributions into account. Doppler shifts can account for between 0.3 to at most 1.0 cm^{-1} shifts for the data considered here. Since this uncertainty is on the order of the quality of the fit across the entire band shown in Figures 12 and 13, corrections at this precision are not warranted. Scattering and size distribution effects can also alter the bands (Tielens et al. 1991). However, since the matches already presented are quite good, we will leave this level of analysis to others, using the optical constants presented in §3.3.

The preceeding arguments point to a picture where the 2140 cm^{-1} band arises from the densest regions of molecular clouds where the production of non-polar species such as O_2, N_2, and CO are favored over polar species such as H_2O. On the other hand, there are at least two distinct regions which can produce H_2O-rich ices and the 2135 cm^{-1} band. In the cloud regions where the H/H_2 ratio is above unity, the production of hydrogenated species such as H_2O is favored over the production of non-polar species on grain surfaces (Tielens and Hagen 1982, d'Hendecourt, Allamandola, & Greenberg 1985). Here, provided the grains are cold enough, CO

and other simple non-polar species can freeze out along with the H_2O (e.g. Sandford & Allamandola 1990a). H_2O-rich ices can also be produced in the warm protostellar regions by the "distillation" of interstellar ices. In this case, the H_2O-rich ices will not be the result of an ongoing, continuous process, but rather they will be all that remains as the ices warm and the more volatile, non-polar species sublime. Consequently, these H_2O-rich ices are most probably different in character from those produced in the $H/H_2 > 1$ regions within the body of the cloud. The prominence of spectral features arising from species such as XCN and CH_3OH toward W33A suggest that most of the extinction toward this object arises from a very dense, warm region close to the source. Here, various processes including UV photolysis will drive a very different chemistry from that in the quiescent cloud regions and these H_2O-rich ices (Bernstein et al. 1995) and their photoproducts are likely to be important feedstock species in protostellar nebulae. Charnley (1996) has recently developed a very interesting model of the gas-grain chemistry in these regions. Thus, it appears that the chemical conditions in protostellar nebula are seemingly at odds with the models of the solar nebula which assume that most of the C is in CO and CH_4, and not CH_3OH.

5.1. *Interstellar N_2 and O_2 Abundances and Depletions*

In order to avoid confusion with contributions from the species in the polar, H_2O-rich fraction of the ice, we restrict the following discussion to the non-polar component in quiescent regions of dense clouds. We believe that this provides a reasonable measure of the non-polar species' abundance along the entire line of sight since depletions of significant amounts (more than 10%) of non-polar species diluted in the H_2O-rich component can be ruled out by the absence of a very prominent high frequency feature near 2150 cm^{-1} in the interstellar spectra (§4.2.).

The calculations described below are based on a non-polar interstellar ice composition of $N_2:O_2:CO_2:CO = 1:5:{}^1/_2:1$. We have selected this composition because it provides a good fit to the interstellar feature (see §4.4) and because it has molecular abundances that are similar to those predicted for quiescent cloud environments by the early chemical models which took both gas-

phase and ice grain processes into account. For example, the time-dependent treatment of d'Hendecourt, Allamandola, and Greenberg (1985) predicted grain mantles dominated by O_2 (43%), CO (30%), N_2 (10%), and CO_2 (8%) in the high density, high extinction regions of dense clouds. Similarly, the equilibrium treatment of Tielens and Hagen (1982) predicted a mantle composition of roughly 58% O_2, 40% CO, and a few percent of CO_2, H_2O, and N_2 in the highest density regions. While these models were quite simple by today's standards, the observations support the basic assumptions involved and will hopefully encourage the inclusion of species such as N_2 and O_2 in the more sophisticated current treatments.

N_2, O_2, and CO_2 are certainly not the only potentially important non-polar interstellar species in these cloud regions. H_2 is likely to be orders of magnitude more abundant than any of the molecules considered here. We rule out H_2 as playing an important role in these non-polar ices for two reasons. First, it is too volatile. While H_2 has been detected frozen in H_2O-rich interstellar ices (Sandford et al. 1993), its binding energy to these non-polar species is such that it would not condense in significant amounts on interstellar grain surfaces. Second, even if some were trapped in these ices, it would not perturb the lattice sufficiently to produce the band broadening required since it is smaller than N_2, O_2, and CO_2. Another plausible species is CH_4. Absorption attributed to frozen CH_4 has been detected toward NGC 7538 IRS 9 and possibly toward W 33 A and NGC 7538 IRS 1 (Lacy et al. 1991). It may even be comparable in abundance to solid CO. Nonetheless, we rule this out as a significant player since it seems the highest abundances with respect to frozen CO are along lines of sight mostly associated with H_2O-rich ices such as W33A. The clearest detection is toward NGC 7538 IRS 9, and here the ratio of solid CO to solid CH_4 is 8. Observations probing the abundance of frozen CH_4 relative to that of frozen H_2O and CO along several other lines of sight toward embedded objects and background stars will place important additional constraints on the ice composition and chemistry of these two regions. Interestingly, Sandford et al. (1988) show that when CH_4 is the dominant constituent, the CO feature falls at 2137 cm^{-1}, very close to the position in H_2O-rich ices. It is too narrow (FWHM = 2-3 cm^{-1}), however, to account for the interstellar feature associated with the polar-component.

Table 8 presents estimates of the O_2 and N_2 solid state column densities and abundances relative to H along the lines of sight to several embedded objects and background field stars. The column densities were derived from those of solid CO, assuming that the ratio of N_2:O_2:CO_2:CO is equal to 1:5:$^1/_2$:1. It should be kept in mind that these assumed relative abundances serve as approximations only. While the relative concentration of CO_2 is fairly well constrained by our spectral matches (any more and it produces a feature that is too broad and too blue), the relative amounts of N_2 and O_2 are not as strongly constrained. For example, our four component ices contain somewhat more O_2 than predicted would be present based on the simple models of Tielens and Hagen (1982) and d'Hendecourt et al. (1985) and our experiments do not preclude the possibility that ices containing smaller amounts of O_2 can still provide a good fit to the interstellar feature. The H abundances were calculated from the standard dust-to-gas conversion $N_H = A_v$ (1.9×10^{21} cm^{-2} mag^{-1}), using extinction (A_v) values published for these objects. The cosmic abundance values, in units of ppm with respect to H, which were adopted for this calculation are O = 480, N = 60, and C = 250. These numbers take into consideration the recent cosmic abundance revisions reported by Witt and Snow (1996), Mathis (1996), and Cardelli et al. (1996).

Within the framework of the assumptions described above, the abundances listed in the table indicate that available interstellar N in the form of frozen N_2 along the lines of sight probed towards background stars lies in the 15-70% range, with an average of about 35%. For the embedded objects, this is reduced to a range of 1-30% with an average of about 10%. N_2 and CO are likely to have similar gas/grain distributions in the quiescent regions because they have very similar heats of vaporization and N_2 is unreactive. Thus, since approximately 40% of the CO is depleted onto grains in quiescent cloud regions (Chiar et al. 1994, 1995), a similar relationship probably holds for N_2. Therefore, in the quiescent regions where an average of 35% of the available N is in frozen N_2, the implication is that as much as 70% of the *total* available N is in N_2 (gas + ice).

The amount of O tied up in frozen O_2 lies in the 1-45% range toward background sources (average $\approx$ 20%), and lies between 1 and 20% for embedded objects (average $\approx$ 10%). The amount of oxygen tied up in frozen CO and CO_2 lies between 2 and 10% of the total O in quiescent

regions, and on the order of 0.2-5% for lines of sight toward embedded objects. Since nearly 40% of the total amount of O available is thought to be tied up in refractory grain materials such as silicates (Cardelli et al. 1996), this implies that nearly half of the O available in the gas could be tied up in O_2 along some lines of sight [although we remind the reader that the estimates for O_2 are likely to be upper limits (see above)].

Lastly, these calculations imply that the fraction of carbon tied up in frozen CO and CO_2 lies in the 3 to 13% range toward field stars and between 0.2-6% toward embedded objects.

We would remind the reader that our assumed non-polar composition of N_2:O_2:CO_2:CO = 1:5:$^1/_2$:1 is probably not unique with regards to its ability to fit the interstellar CO feature. Similar quality fits to the interstellar feature can probably be made with a range of non-polar compositions. For example, the features produced by N_2:O_2:CO = 1:5:1 and N_2:H_2O:CO = 5:1:5 ices (see Figure 12) suggest that it is possible that minor amounts of H_2O may carry out the same spectral function as larger amounts of O_2. Thus, it might be possible to obtain a comparably good fit to the interstellar feature by replacing the N_2:O_2:CO_2:CO = 1:5:$^1/_2$:1 non-polar component with an ice of the form N_2:H_2O:CO_2:CO. Thus, the cosmic abundances summarized in Table 8 should not be taken as exact, but should serve as a guide only. Furthermore, we remind the reader that the previous discussion relates only to the cosmic abundance contributions made by the *non-polar* fraction of the CO-bearing ices. The *polar*, H_2O-rich ice component will also provide significant contributions to the cosmic inventory. As shown in Figure 13, the contribution of C and O due to the polar ices can be comparable to those from the non-polar ices, especially along lines of sight towards embedded objects.

In summary, based on the assumption that the 2140 cm^{-1} CO band is produced by a non-polar ice having a composition of N_2:O_2:CO_2:CO = 1:5:$^1/_2$:1, it appears that most of the interstellar N and a significant fraction of the interstellar O in the quiescent regions of dense molecular clouds are in the form of N_2 and O_2. These two molecular components appear to be far more important in quiescent regions of the cloud than along lines of sight to embedded objects. Given that the spectra of embedded objects also contain variable, but significant, spectral contributions from foreground

quiescent cloud material, but still show substantial reductions in implied N_2 and O_2, suggests that the ices in the vicinity of embedded objects are significantly different from those in more typical regions in dense clouds.

This may also have some implications for our understanding of the conditions in the solar nebula and the composition of icy bodies at large distances from the protostar. For example, if these objects were formed at large enough distances that the temperatures never rose much above 30 K, these icy planetessimals would might well contain significant amounts of N_2 and O_2. Cometary outbursts at large heliocentric distances such as that recently reported for Comet Hale-Bopp are often attributed to the release of volatiles such as CO. If comets contain some of the interstellar ices that were present prior to the formation of the solar system, O_2 and N_2 should certainly be present. These too should be considered, as they will also drive releases at low temperatures.

5.2. *Photoproducts of Non-Polar Ices*

Since N_2, O_2, and CO_2 are likely to be important interstellar ice components, the products formed by the energetic processing of these ices are of interest. The results presented in §3.2 show that N_2O, O_3, and CO_3 might also be important interstellar ice components in cold ($T < 30$ K) regions exposed to radiation. Figures 8 and 9 show that the strongest N_2O bands fall near 2235 and 1291 cm^{-1} (4.474 and 7.746 μm) in these non-polar ices. Similarly, the strongest O_3 and CO_3 bands are at about 1039 and 2041 cm^{-1} (9.625 and 4.900 μm), respectively. NO and NO_2 might also be important as well. The strongest absorptions associated with these two species fall between 1620 to 1610 cm^{-1} (6.17 to 6.21 μm) and near 1860 cm^{-1} (5.38 μm), respectively. Searching for these absorptions in appropriate ISO spectra will be important for understanding the chemistry in those regions and will provide important insight into the disposition of interstellar N and O. For example, the detection of these species along lines of sight probing quiescent regions of dense molecular clouds will support the hypothesis that photochemistry is important even in the densest regions of molecular clouds, while the non-detection would argue against this. It will also be important to probe lines of sight that are dominated by the protostellar environment such as

represented by W33A. Since the CO profile is not dominated by the non-polar component in the spectrum on W33A, one would anticipate that species such as N_2O, O_3, and CO_3 would not be as abundant with respect to the ice features associated with more polar, less volatile species such as H_2O, XCN, CH_3OH, and so on toward this object. Of course, N_2O, O_3, and CO_3, if present in the gas, can freeze onto grains at temperatures above 30 K. Thus, band positions and profiles will be very important diagnostic tools in sorting out the subtleties of the chemical processes at play in these very different environments. Further studies of of non-polar ice photochemistry will be warranted if ISO detects any of these photoproduct bands.

Other very important results of our photolysis studies are that: (i) XCN was not formed in *any* of our experiments, and (ii) there are serious reservations concerning the detection of photoproducts that contain a *single* nitrogen atom. These are especially significant in light of the questions surrounding the identity and formation of the species designated XCN, a common photoproduct in laboratory ices containing a photolytic source of free N-atoms such as NH_3 (cf. d'Hendecourt et al. 1986; Bernstein et al. 1995). XCN is thought to be responsible for the interstellar 2165 cm^{-1} band (Lacy et al. 1984). These experiments rule out the suggestion made in Tegler et al. (1995) that interstellar XCN is produced by the photolysis of N_2-rich ices. Taken together, these results support the hypothesis made by Lacy et al.(1984) and Teglar et al. (1995) that XCN is somehow associated with the protostellar environment, and is not a general characteristic of dense clouds. If this proves to be the case, careful characterization of the types of ices along lines of sight dominated by the protostellar environment versus those associated with more quiescent regions may well provide important constraints into the conditions prevalent in the early protosolar nebula.

6. SUMMARY

This paper presents the results of laboratory work in which the infrared spectral properties of CO frozen in mixed molecular ices containing O_2, N_2, CO_2, and H_2O were studied. The precise position, FWHM, and profile of the CO stretching fundamental near 2140 cm^{-1} depends

sensitively on the composition of the ice, the conditions under which it formed, and its subsequent thermal and radiation history. The optical constants (real and imaginary parts of the index of refraction) in the region of the solid CO feature are reported for several of the ices studied.

This project was undertaken to gain insight into the nature of the ices responsible for the 2140 cm^{-1} interstellar, frozen CO feature which is characteristic of lines of sight through quiescent regions of dense molecular clouds. Comparison of the laboratory data with astronomical spectra show that CO frozen in O_2 and N_2 ices alone cannot account for the 2140 cm^{-1} component. For N_2 and O_2-rich ices, the feature is too narrow, the profile doesn't match, and the band falls at too low a frequency. Although mixtures containing comparable amounts of O_2, N_2, and CO do an excellent job of accounting for the low frequency portion of the interstellar feature, they cannot reproduce the peak position or high frequency side. The band is far too narrow if there is more than two to three times as much N_2 or O_2 as CO. The band position and width in the N_2:O_2:CO = 1:1:1 and 1:5:1 ices both produce narrow CO bandwidths, and peak about 1 cm^{-1} to the red of the interstellar feature. Thus, while N_2 and O_2 mixtures containing CO can contribute to the interstellar feature, an additional component is required to provide the high frequency absorption. Of the non-polar materials studied, CO_2 is the only one that produces the necessary high frequency absorption. Concentration studies on four component mixtures containing N_2,O_2,CO_2, and CO show that the amount of CO_2 in the ice cannot exceed the amount of CO if a good fit to the interstellar 2140 cm^{-1} CO feature is to a obtained. Of the ices we have studied, a composition of N_2:O_2:CO_2:CO = 1:5:$^1/_2$:1 provided the best fit to the 2140 cm^{-1} interstellar feature. This match is good both before and after UV photolysis and at all temperatures between 12 and 30 K.

While our experiments do not fully constrain the O_2 concentration needed in four component non-polar ices to provide a good match to the interstellar 2140 cm^{-1} feature, the good fit provided by our N_2:O_2:CO_2:CO = 1:5:$^1/_2$:1 ice allows us to make an estimate of how much material is tied up in the non-polar ice component. Applying cosmic abundance constraints and assumed relative abundances of N_2:O_2:CO_2:CO = 1:5:$^1/_2$:1, we find that between 15-70% (average $\approx$ 35%) of the available interstellar N could be in the form of frozen N_2 along the lines of sight towards

background stars, i.e. in the quiescent regions in clouds. This is reduced to about 1-30% (average ≈ 10%) for lines of sight towards embedded objects. Oxygen in the form of O_2 lies in the 1-45% range (average ≈ 20%) toward background sources and between 1 and 20% (average ≈ 10%) toward embedded objects. The amount of oxygen tied up in frozen CO and CO_2 would then lie in the 2-10% range towards background stars and between about 0.2-5% towards protostars. Similarly, between 3 to 13% of the carbon would then be tied up in frozen CO and CO_2 toward field stars, and 0.2 to 6% toward embedded objects. These numbers imply that (i) most of the cosmic N is in the form of N_2, (ii) in quiescent regions of dense clouds a significant fraction of the available O in the gas is in O_2, and (iii) the ices surrounding embedded objects have a very different character from those found in quiescent regions.

The infrared activity of the N_2 stretching vibration is induced in these ices, producing a band at 2328 cm^{-1} (4.296 μm) which corresponds to that previously observed in frozen N_2. Similarly, the O_2 stretching vibration is also induced in these ices and it produces an absorption feature near 1549 cm^{-1} (6.456 μm).

Photolysis of a number of the ices produced a variety of new species including CO_2, N_2O, O_3, CO_3, HCO, H_2CO, and possibly NO and NO_2. The UV photolysis of N_2-rich ices appears to be very inefficient at breaking N-N bond and photolysis of these mixtures did *not* produce XCN. The suggestion of Tegler et al. (1995) that XCN is produced by the photolysis of CO in N_2-rich ices is therefore incorrect. The identification of N_2O, CO_3, and O_3 among the common products of photolysis of ices containing O_2, N_2, CO_2, and CO is important. It provides observers with new absorption bands to search for, bands whose presence or absence will place constraints on the conditions and chemistry occurring in dense clouds. Detection of interstellar solid N_2O bands would indicate the presence of N_2, while the strength of the O_3 bands would give an indication of the importance of O_2.

We conclude this paper by repeating a quote from Allamandola and Sandford (1988) concerning the interstellar solid state CO feature, a quote which is as pertinent today as it was nearly a decade ago when it was written: "It is important to realize that being able to determine peak

position to an accuracy of about 0.2 cm^{-1} at a frequency of 2140 cm^{-1} implies that an observational resolution of 1 part of 10^4 is required to fully extract the information carried by this band. No other interstellar ice feature we are presently aware of requires such resolution for analysis. In most cases 1 part in 10^3 is sufficient. The unique combination of the ability to measure the interstellar CO feature with such precision, in conjunction with the high sensitivity of the solid state CO band position and profile on the nature of the solid, provides far more insight into the nature of the cloud (solid state properties as well as gas-phase chemistry) than even the most optimistic analog aficionados anticipated a few years ago."

ACKNOWLEDGMENTS

We very gratefully acknowledge Max Bernstein for many helpful scientific discussions, help with laboratory procedures, and generously measuring all of the four component ices reported here. We are also especially grateful to Dr. S. Laursen, Professor of Chemistry at Kalamazoo College, for her suggestion that Jamie Elsila carry out her Senior Research project with us at NASA-Ames, and for her encouragement throughout this project. As always, we also acknowledge Bob Walker for his excellent technical support. This work was supported by NASA grants 185-52-12-04 (Exobiology Program) and 452-33-93-03 (Origins of the Solar Systems Program).

REFERENCES

Allamandola, L. J., & Sandford, S. A. 1988 in *Dust in the Universe*; eds. M. E. Bailey, & D. E. Williams, (Cambridge: Cambridge University Press), 229.

Allamandola, L. J., Sandford, S. A., & Valero, G. J. 1988, Icarus, 76, 225

Allamandola, L. J., Sandford, S. A., Bernstein, M. B., & Elsila, J. 1996, in preparation

Bergmen, M. S., Schuh, D., Sceats, M. G., & Rice, S. A. 1978, J. Chem. Phys., 69, 3477.

Bernstein, M. P., Sandford, S. A., Allamandola, L. J., Chang, S., & Scharberg, M. A. 1995, ApJ, 454, 327

Bertie, J. E., Labbe. H. J., & Whalley, E. 1969, J. Chem. Phys., 50, 4501.

Bohn, R. 1993, Astrochemistry Laboratory, NASA Ames Research Center, unpublished results.

Bohn, R. B., Sandford, S. A., Allamandola, L. J., & Cruikshank, D. P. 1994, Icarus, 111, 151

Cardelli, J. A., Meyer, D. M., Jura, M., & Savage, B. D. 1996, preprint

Charnley, S. 1996, preprint

Chiar, J. E., Adamson, A. J., Kerr, T. H., & Whittet, D. C. B. 1994, ApJ, 426, 240

Chiar, J. E., Adamson, A. J., Kerr, T. H., & Whittet, D. C. B. 1995, ApJ, 455, 234

d'Hendecourt, L. B., Allamandola, L. J., & Greenberg, J. M., 1985, A&A, 152, 130

d'Hendecourt, L. B., Allamandola, L. J., Grim, R. J. A., & Greenberg, J. M. 1986 A&A, 158, 119

d'Hendecourt, L. B., & Allamandola, L. J. 1986, A&ASS, 64, 453.

Dows, D. A. 1957, J. Chem. Phys., 26, 745

Dubost, H., Charneau, R., & Harig, M. 1982, Chem. Phys., 69, 389

Ehrenfreund, P., Breukers, R., d'Hendecourt L., & Greenberg, J. M. 1992, A&A, 260, 431

Eiroa, C., & Hodapp, K. W., 1989, A&A, 210, 345

Ewing, G. E., Thompson, W. E., & Pimentel, G. C. 1960, J. Chem. Phys, 32, 927

Fately, W. G., Bent, H. A., & Crawford, B., 1959, J. Chem. Phys. 31, 204

Geballe, T. R. 1986, A&A, 162, 248

Gerakines, P. A., Schutte, W. A., Greenberg, J. M., & van Dishoek, E. F., 1995, A&A 296, 810

Grundy, W. M., Schmitt, B. & Quirico, E. 1993, Icarus, 105, 254

Hagen, W., Allamandola, L. J., & Greenberg, J. M. 1980, A&A, 86, L3

Hagen, W., Tielens, A. G. G. M., & Greenberg, J. M. 1981, Chem. Phys., 56, 367.

Hallam, H. E., & Scrimshaw, G. F. 1973, in Vibrational Spectroscopy of Trapped Species, Hallam, H. E. (ed.), (John Wiley and Sons, New York), p. 11.

Herzberg, G. H. 1955, Mem. Soc. Roy. Liege, 15, 291

Hudgins, D. M., Sandford, S. A., Allamandola, L. J., & Tielens, A. G. G. M. 1993, ApJSS, 86, 713

Hudgins, D. M., Sandford, S. A., Allamandola, L. J., & Tielens, A. G. G. M. 1994, *The AAS CD-ROM Series*, Volume 1, (expanded version of the tables in ApJSS, 86, 713

Jiang, G. J., Person, W. B., & Brown, K. G. 1975, J. Chem. Phys., 62, 1201

Kerr, T. H., Adamson, A. J., & Whittet, D. C. B. 1991, MNRAS, 251, 60p

Lacy, J. H., Baas, F., Allamandola, L. J., Persson, S. E., McGregor, P. J., Lonsdale, Carol J., Geballe, T. R., & van de Bult, C. E. P. M. 1984, ApJ., 276, 533

Lacy, J. H., Carr, J., Evans, N., Baas, F., Achterman, J., & Arens, J. 1991 ApJ, 376, 556

Latter, W. B., Radford, S. J. E., Jewell, P. R., Mangum, J., & Bally, J. 1996, eds. *CO: Twenty-Five Years of Millimeter Wave Spectroscopy* (Dordrecht: Kluwer)

Leger, A., Gauthier, S., Défourneau, D., & Rouan, D. 1983, A&A, 117, 164.

Leung, C. M. 1976, ApJ, 209, 75

Löwen, H. W., Bier, K. D., & Jodl, H. J. 1990, J. Chem. Phys., 93, 8565

Mathis, J. S., 1996, preprint

Milligan, D. E. & Jacox, M. E. 1971, J. Chem. Phys., 54, 927

Mitchell, G. F., Allen, M., & Maillard, J. P. 1988, ApJ, 333, L55

Mitchell, G. F., Maillard, J. P., Allen, M., Beer, R., & Belcourt, K. 1990, ApJ, 363, 554

Moll, N. G., Clutter, D. R., & Thompson, W. E. 1960, J. Chem. Phys., 45, 4469

Palumbo, M. E., & Strazzulla, G. 1993, A&A, 269, 568

Pearl, J., Ngoh, M., Ospina, M., & Khanna, R. 1991, J. Geophys. Res., 96, 17477.

Roux, J. A., Wood, B. E., Smith, A. M., & Plyler, R. R. 1980, AEDC-TR-79-81 (AD-A088269).

Sandford, S. A., & Allamandola, L. J. 1990a, Icarus, 87, 188

Sandford, S. A., & Allamandola, L. J. 1990b, ApJ, 355, 357

Sandford, S. A., & Allamandola, L. J. 1993, ApJ, 417, 815

Sandford, S. A., Allamandola, L. J., Tielens, A. G. G. M. & Valero, G. J. 1988, ApJ, 329, 498

Sandford, S. A., Allamandola, L. J., & Geballe, T. R. 1993, Science, 262, 400

Sandford, S. A. 1996a, Meteoritics & Planetary Sci., in press, July issue

Sandford, S. A., 1996b, in Polarimetry of the Interstellar Medium, eds. W. Roberge & D. C. B. Whittet, in press

Schmitt, B., Greenberg, J. M., & Grim, R. J. A. 1989, ApJ, 340, L33

Schutte, W. A., Allamandola, L. J., & Sandford, S.A. 1993, Icarus, 104, 114

Smith, A. L., Keller, W. E., & Johnston, H. L. 1950, Phys. Rev., 79, 728

Snow, T. P., & Witt, A. N. 1995, Science, 270, 1455

Soifer, B. T., Puetter, R. C., Russell, R. W., Willner, S. P., Harvey, P. M., & Gillett, F. C. 1979, ApJ, 232, L53

St. Louis, R. V. & Crawford, B. 1965, J. Chem. Phys., 42, 857

Tegler, S. C., Weintraub, D. A., Rettig, T. W., Pendleton, .J., Whittet, D. B., & Kulesa, C. A. 1995, ApJ, 439, 279

Tielens, A. G. G. M, & Hagen, W. 1982, A&A, 114, 245

Tielens, A. G. G. M., Tokunaga, A. T., Geballe, T. R., & Baas, F. A. 1991, ApJ, 381, 181

Tryka, K. A., Brown, R. H., & Anicich, V. 1995, Icarus, 116, 409

Warren, S. G. 1986, App. Optics, 25, 2650.

Whittet, D. C. B., 1993, in Dust and Chemistry in Astronomy, eds. T. J. Millar & D. A. Williams, (Cambridge: Cambridge Univ. Press), 9

Whittet, D. C. B., Longmore, A. J., & McFadzean, A. D. 1985, MNRAS, 216, 45p

Whittet, D. C. B., Adamson, A. J., Duley, W. W., Geballe, T. R., & McFadzean, A. D. 1989, MNRAS, 241, 707

Whittet, D. C. B., Smith, R. G., Adamson, A. J., Aitken, D. K., Chiar, J. E., Kerr, T. H., Roche, P. F., Smith, C. H., & Wright, C. M. 1996, ApJ, 458, 363

Wilson, R. W., Jefferts, K. B., & Penzias, A. A. 1971, ApJ, 161, L43.

Wood, B. E., & Roux, J. A. 1982, J. Opt. Soc. Am., 72, 720.

TABLE 1 - Mixed-Molecular CO-Containing Ices Considered in this Study[a]

N_2:CO	N_2:H_2O:CO	N_2:O_2:CO
(100:1)	100:1:1	(1:1:1)
25:1	(19:1:1)	1:5:1
(2:1)	10:1:1	
(1:20)	5:1:1	N_2:CO_2:CO
	(2:1:1)	1:1:1
O_2:CO	5:1:5	1:5:1
20:1	10:1:10	
		N_2:O_2:CO_2:CO
CO_2:CO		1:3:5:1
20:1		1:5:$^3/_2$:1
		(1:5:$^1/_2$:1)

(a) Mixtures in parentheses were also photolyzed.

TABLE 2 - Peak Positions and FWHM of the CO Feature in N_2:CO Mixed-Molecular Ices as a Function of Temperature[a]

Ice Composition and Temperature	CO Position (cm^{-1})	FWHM (cm^{-1})
N_2:CO = 100:1		
12 K	2139.6	1.1
25 K	2139.6	1.0
32 K	2139.6	1.1
N_2:CO = 25:1		
12 K	2139.7	1.2
30 K	2139.7	1.3
33 K	2137.8	~8
N_2:CO = 2:1		
12 K	2138.7	2.6
30 K	2138.7	2.5
32 K	2138.7	2.3
34 K	2140.1	~8
N_2:CO = 1:20		
12 K	2138.2	2.6
25 K	2138.2	2.3
32K	2138.7	2.0
34 K	2139.2	7.0

(a) All ices deposited at 12 K and then warmed to the indicated temperatures.

TABLE 3 - Peak Positions and FWHM of the CO Feature in N_2- and H_2O-Containing Mixed-Molecular Ices[a,b]

Ice Composition and Temperature	CO Position (cm^{-1})	FWHM (cm^{-1})
N_2:H_2O:CO = 100:1:1		
12 K	2139.6 (2148.4)	1.2 (1.2)
25 K	2139.7 (2146.9)	0.9 (1.4)
30 K	2139.6 (2146.9)	1.1 (1.3)
35 K	2141.1 (2152.5)	10.0 (8.3)
N_2:H_2O:CO = 19:1:1		
12 K	2139.6 (2147.4)	1.6 (2.3)
25 K	2139.6 (2149.7)	1.4 (4.0)
30 K	2139.6 (2150.7)	1.4 (5.3)
35 K	2139.6 (2150.7)	1.3 (6.7)
40 K	2136.2 (2151.8)	11.0 (15.0)
N_2:H_2O:CO = 10:1:1		
12 K	2139.7 (2147.3)	3.0 (7.0)
25 K	2139.7 (2147.4)	2.4 (7.4)
30 K	2139.5 (2147.3)	2.4 (7.8)
35 K	2138.8 (2150.1)	10.0 (7.0)
N_2:H_2O:CO = 5:1:1		
12 K	2139.6 (2148.4)	3.6 (7.2)
25 K	2139.6 (2148.8)	3.5 (7.2)
30 K	2139.2 (2149.8)	3.4 (8.0)
35 K	2138.3 (2149.7)	7.4 (>10)
N_2:H_2O:CO = 2:1:1		
12 K	2139.2 (2148.4)	5.3 (7.2)
25 K	2139.2 (2148.8)	5.3 (7.2)
30 K	2139.2 (2149.2)	4.8 (7.0)
35 K	2138.2 (2149.3)	8.5 (8.0)
N_2:H_2O:CO = 5:1:5		
12 K	2139.1 (2148.8)	4.7 (5.4)
25 K	2139.1 (2148.8)	4.0 (5.4)
30 K	2138.7 (2148.8)	4.0 (5.4)
35 K	2139.1 (2150.0)	9.0 (4.7)
N_2:H_2O:CO = 10:1:10		
12 K	2139.1	2.8
25 K	2138.7	2.8
30 K	2138.7	2.7
35 K	2138.6	~10

(a) Numbers in parenthesis correspond to the weaker feature on the high frequency side of the main feature (see Figure 3).
(b) All ices deposited at 12 K and then warmed to the indicated temperatures.

TABLE 4 - Peak Positions and FWHM of the CO Feature in O_2- and CO_2-Containing Mixed-Molecular Ices With and Without N_2 [a]

Ice Composition	Ice Temperature	CO Position (cm^{-1})	FWHM (cm^{-1})
N_2:O_2:CO = 1:1:1	12 K	2139.2	4.0
	25 K	2139.2	3.7
	30 K	2138.7	3.3
	35 K	2138.2	6.0
N_2:O_2:CO = 1:5:1	12 K	2138.7	3.9
	25 K	2139.2	4.2
	30 K	2139.2	3.6
	35 K	2138.7	2.7
O_2:CO = 20:1	12 K	2135.8	3.7
	25 K	2136.3	3.2
	30 K	2136.3	2.3
	35 K	2139.6	2.7
N_2:CO_2:CO = 1:1:1	12 K	2139.6	2.3
	25 K	2139.6	2.3
	30 K	2139.6	2.5
	35 K	2139.7	7.4
	40 K	2140.7	8.4
	70 K	2139.6	8.0
N_2:CO_2:CO = 1:5:1	12 K	2141.5	9.6
	25 K	2141.6	9.3
	30 K	2141.6	9.3
	35 K	2141.6	9.2
	70 K	2139.6	7.6
CO_2:CO = 20:1	12 K	2139.2	4.8
	35 K	2139.2	5.0
	50 K	2139.2	4.2
N_2:O_2:CO_2:CO = 1:3:5:1	12 K	2142.7	8.5
N_2:O_2:CO_2:CO = 1:5:1.5:1	12 K	2142.1	6.9
	20 K	2142.1	6.9
	25 K	2142.3	6.3
	30 K	2142.5	6.3
	35 K	2143.4	8.4
N_2:O_2:CO_2:CO = 1:5:0.5:1	12 K	2141.0	7.1
	20 K	2141.4	6.9
	25 K	2141.6	5.9
	30 K	2141.6	6.8
	35 K	2143.2	8.1

(a) All ices deposited at 12 K and then warmed to the indicated temperatures.

TABLE 5 - The Identification of Features Appearing Upon the UV Photolysis of Various Ices Containing N_2, H_2O, CO_2, and CO[a]

Identification	Band Position (cm^{-1})							Reference
	N_2:CO 100:1	N_2:CO 2:1	N_2:CO 1:20	N_2:H_2O:CO 20:1:1	N_2:H_2O:CO 2:1:1	N_2:O_2:CO 1:1:1	N_2:O_2:CO_2:CO 1:5:0.5:1	
CO_2	(b)	3708.7 vw	3706.4 vw	(c)	(c)	3705.1 w	(d) w	Sandford et al. 1990
CO_2	(b)	3603.2 vw	3601.7 vw	(c)	(c)	3600.9 w	(d) w	Sandford et al. 1990
CO_2	2346.1 m	2347.3 m	2346.7 m	2348.8 s	2345.3 s	2347.0 s	(d) vs	Sandford et al. 1990
$^{13}CO_2$		2281.7 vw	2281.1 vw	2282.7 w	2279.2 w	2279.1 w	(d) w	Sandford et al. 1990
N_2O	2234.7 m	2235.0 w		2235.6 w	2234.5 w	2234.1 w-m	2232.0 s	Dows 1957
O_3						2108.0 w	2109.3 w	Bohn 1993
CO_3						2041.4 w	2042.2 s	Moll et al. 1960
CO_3						1881.1 vw	1888.4 w	Moll et al. 1960
HCO				1858.8 vw	1856.4 m			Milligan & Jacox 1971
?					1788.6 w			
H_2CO					1721.3 m			Schutte et al. 1993
NO_2, ?	1606.9 m	1604.0 vw				1607.4 vw	1607.9 w	St. Louis & Crawford 1965
H_2CO					1499.3 w			Schutte et al. 1993
N_2O	1290.7 w	1290.4 vw		1290.6 w	1287.0 vw	1289.8 w	1286.6 w	Dows 1957
H_2CO					1247.2 vw			Schutte et al. 1993
?							1235 vw	
O_3						1104.0 vw		Bohn 1993
H_2CO					1147.6 vw			Schutte et al. 1993
HCO					1092.1 w			Milligan & Jacox 1971
O_3	1040.8 m	1041.0 w	1038.6 w	1039.6 w	1037.7 w	1038.0 m	1037.0 vvs	Bohn 1993
CO_3						975.0 vw	976 w	Dows 1957
O_3						703.4 w	703.4 w	Bohn 1993
CO_2	661.9 m	661.9 m	662.0 w	662.3 m	663.9 m	662.3 m	(d) s	Sandford et al. 1990

(a) vvs = very very strong, vs = very strong, s = strong, m = moderate, w = weak, vw = very weak, vvw = very, very weak with respect to the very strong CO absorption after 3 hours of photolysis.
(b) Weak absorptions obscured by bands due to minor contaminant H_2O.
(c) Obscured by H_2O bands.
(d) Total CO_2 band areas increase by a factor of ~2 upon photolysis, implying CO_2 production.

TABLE 6 - CO Peak Position and FWHM at 12 K Before and After UV Photolysis

Ice Composition	Prephotolysis CO Position (FWHM) (cm^{-1})	Postphotolysis CO Position (FWHM) (cm^{-1})
N_2:CO = 100:1	2139.6 (1.1)	2139.6 (1.1)
N_2:CO = 2:1	2138.7 (2.6)	2139.2 (3.0)
N_2:CO = 1:20	2138.2 (2.6)	2139.7 (2.6)
N_2:H_2O:CO = 19:1:1	2139.6 (1.6)	2139.6 (1.6)
N_2:H_2O:CO = 2:1:1	2139.2 (5.3)	2139.2 (5.3)
N_2:O_2:CO = 1:1:1	2139.2 (4.0)	2139.2 (6.0)
N_2:O_2:CO_2:CO = 1:5:0.5:1	2141.0 (7.1)	2141.1 (7.7)

TABLE 7a - Optical Constants

	N_2:O_2:CO_2:CO =1:5:0.5:1 (n_o = 1.24) (d = 1.85x10^{-5} cm)		H_2O:CO =20:1 (n_o = 1.32) (d = 4.35x10^{-5} cm)		N_2:CO_2:CO =1:5:1 (n_o = 1.22) (d = 6.5x10^{-6} cm)		N_2:H_2O:CO =5:1:5 (n_o = 1.27) (d = 2.56x10^{-5} cm)		N_2:O_2:CO =1:5:1 (n_o = 1.25) (d = 8.1x10^{-5} cm)	
Freq. (cm^{-1})	***n***	***k***	***n***	***k***	***n***	***k***	***n***	***k***	***n***	***k***
2065.4	1.2550	0.0003	1.3512	0.0065	1.2917	0.0001	1.2852	0.0009	1.2578	0.0005
2073.1	1.2561	0.0007	1.3521	0.0070	1.2931	0.0001	1.2872	0.0009	1.2585	0.0005
2080.9	1.2569	0.0007	1.3531	0.0077	1.2962	0.0006	1.2904	0.0012	1.2599	0.0006
2088.6	1.2585	0.0017	1.3540	0.0087	1.2997	0.0003	1.2964	0.0037	1.2622	0.0019
2096.3	1.2576	0.0029	1.3547	0.0088	1.3019	0.0027	1.2919	0.0014	1.2607	0.0009
2098.7	1.2581	0.0020	1.3553	0.0089	1.3013	0.0024	1.2952	0.0015	1.2618	0.0008
2101.1	1.2588	0.0019	1.3556	0.0091	1.3043	0.0002	1.2974	0.0011	1.2630	0.0008
2103.5	1.2594	0.0014	1.3563	0.0090	1.3061	0.0000	1.2999	0.0006	1.2639	0.0007
2105.9	1.2604	0.0018	1.3567	0.0095	1.3075	0.0009	1.3023	0.0008	1.2649	0.0009
2108.3	1.2615	0.0011	1.3575	0.0094	1.3101	0.0007	1.3057	0.0003	1.2662	0.0007
2110.8	1.2626	0.0013	1.3582	0.0097	1.3114	0.0002	1.3088	0.0007	1.2677	0.0008
2113.2	1.2637	0.0016	1.3589	0.0098	1.3138	0.0010	1.3127	0.0010	1.2693	0.0009
2115.6	1.2651	0.0016	1.3600	0.0099	1.3153	0.0015	1.3167	0.0000	1.2712	0.0007
2116.5	1.2658	0.0014	1.3604	0.0101	1.3171	0.0017	1.3189	0.0000	1.2721	0.0006
2117.5	1.2666	0.0012	1.3609	0.0100	1.3176	0.0018	1.3213	0.0000	1.2732	0.0007
2118.5	1.2675	0.0010	1.3614	0.0102	1.3186	0.0015	1.3239	0.0000	1.2743	0.0007
2119.4	1.2682	0.0011	1.3621	0.0102	1.3186	0.0007	1.3264	0.0001	1.2753	0.0007
2120.4	1.2696	0.0002	1.3628	0.0104	1.3222	0.0000	1.3293	0.0000	1.2768	0.0007
2121.4	1.2707	0.0014	1.3636	0.0104	1.3234	0.0005	1.3326	0.0000	1.2783	0.0008
2122.3	1.2716	0.0010	1.3646	0.0105	1.3253	0.0013	1.3358	0.0000	1.2798	0.0008
2123.3	1.2731	0.0011	1.3657	0.0107	1.3259	0.0014	1.3397	0.0000	1.2816	0.0008
2124.3	1.2747	0.0002	1.3670	0.0107	1.3279	0.0000	1.3443	0.0000	1.2838	0.0006
2125.2	1.2764	0.0010	1.3685	0.0109	1.3311	0.0004	1.3491	0.0000	1.2862	0.0005
2126.2	1.2782	0.0005	1.3707	0.0113	1.3341	0.0020	1.3549	0.0000	1.2891	0.0008
2127.2	1.2804	0.0008	1.3734	0.0120	1.3344	0.0038	1.3614	0.0000	1.2924	0.0008
2128.1	1.2832	0.0000	1.3760	0.0134	1.3371	0.0000	1.3686	0.0000	1.2960	0.0006
2129.1	1.2864	0.0005	1.3797	0.0158	1.3419	0.0024	1.3781	0.0000	1.3009	0.0006
2130.0	1.2895	0.0006	1.3834	0.0197	1.3449	0.0018	1.3882	0.0000	1.3063	0.0005
2130.5	1.2919	0.0000	1.3860	0.0223	1.3475	0.0028	1.3942	0.0000	1.3099	0.0006
2131.0	1.2947	0.0001	1.3861	0.0255	1.3494	0.0043	1.4013	0.0000	1.3139	0.0005
2131.5	1.2975	0.0008	1.3878	0.0293	1.3516	0.0036	1.4094	0.0000	1.3186	0.0004
2132.0	1.3005	0.0007	1.3884	0.0336	1.3554	0.0028	1.4186	0.0000	1.3242	0.0002
2132.5	1.3041	0.0012	1.3883	0.0385	1.3586	0.0047	1.4289	0.0000	1.3309	0.0002
2132.9	1.3073	0.0009	1.3877	0.0434	1.3624	0.0088	1.4387	0.0000	1.3373	0.0001
2133.4	1.3123	0.0014	1.3865	0.0486	1.3658	0.0110	1.4518	0.0000	1.3472	0.0002
2133.9	1.3183	0.0017	1.3838	0.0535	1.3692	0.0137	1.4676	0.0000	1.3601	0.0006
2134.4	1.3256	0.0033	1.3802	0.0580	1.3729	0.0170	1.4866	0.0000	1.3772	0.0028
2134.9	1.3346	0.0054	1.3760	0.0621	1.3767	0.0215	1.5098	0.0002	1.3996	0.0098
2135.4	1.3469	0.0104	1.3708	0.0656	1.3828	0.0269	1.5390	0.0038	1.4308	0.0273
2135.8	1.3538	0.0190	1.3674	0.0680	1.3831	0.0319	1.5648	0.0110	1.4425	0.0632
2136.3	1.3653	0.0337	1.3592	0.0695	1.3870	0.0385	1.6049	0.0232	1.4565	0.1159
2136.8	1.3724	0.0535	1.3553	0.0697	1.3893	0.0485	1.6529	0.0424	1.4485	0.1737
2137.3	1.3742	0.0781	1.3492	0.0691	1.3901	0.0579	1.7136	0.0702	1.4252	0.2229
2137.8	1.3707	0.1027	1.3434	0.0672	1.3913	0.0683	1.8143	0.1096	1.4018	0.2603
2138.2	1.3578	0.1261	1.3399	0.0644	1.3874	0.0787	1.8704	0.2121	1.3452	0.3011
2138.7	1.3440	0.1436	1.3343	0.0610	1.3857	0.0892	1.9520	0.4344	1.3172	0.3422
2139.2	1.3288	0.1568	1.3326	0.0574	1.3806	0.0985	1.8910	0.7995	1.2451	0.3700
2139.7	1.3105	0.1658	1.3299	0.0533	1.3751	0.1078	1.6565	1.0962	1.1648	0.3622
2140.2	1.2922	0.1714	1.3281	0.0493	1.3680	0.1174	1.3327	1.1738	1.0922	0.3164
2140.7	1.2726	0.1754	1.3268	0.0455	1.3637	0.1264	1.1560	1.0445	1.0605	0.2488
2141.1	1.2500	0.1826	1.3263	0.0419	1.3490	0.1345	0.8035	0.9670	1.0302	0.1729
2141.6	1.2370	0.1846	1.3264	0.0383	1.3411	0.1398	0.7135	0.7309	1.0310	0.1076
2142.1	1.2192	0.1844	1.3272	0.0353	1.3287	0.1427	0.6552	0.4467	1.0495	0.0545
2142.6	1.1956	0.1795	1.3279	0.0327	1.3163	0.1451	0.7025	0.2270	1.0771	0.0209

TABLE 7a - Optical Constants (*continued*)

	N_2:O_2:CO_2:CO =1:5:0.5:1		H_2O:CO =20:1		N_2:CO_2:CO =1:5:1		N_2:H_2O:CO =5:1:5		N_2:O_2:CO =1:5:1	
Freq. (cm^{-1})	***n***	***k***	***n***	***k***	***n***	***k***	***n***	***k***	***n***	***k***
2143.1	1.1721	0.1677	1.3289	0.0304	1.3027	0.1454	0.7870	0.1240	1.1046	0.0061
2143.6	1.1566	0.1492	1.3299	0.0286	1.2978	0.1418	0.8676	0.0717	1.1266	0.0013
2144.0	1.1411	0.1277	1.3316	0.0271	1.2753	0.1384	0.9104	0.0441	1.1402	0.0000
2144.5	1.1350	0.1033	1.3319	0.0260	1.2713	0.1299	0.9690	0.0338	1.1534	0.0000
2145.0	1.1325	0.0805	1.3336	0.0252	1.2619	0.1222	1.0090	0.0305	1.1635	0.0000
2145.5	1.1345	0.0598	1.3347	0.0246	1.2535	0.1136	1.0393	0.0317	1.1714	0.0002
2146.0	1.1433	0.0428	1.3357	0.0243	1.2497	0.1046	1.0644	0.0368	1.1780	0.0004
2146.4	1.1488	0.0301	1.3371	0.0242	1.2419	0.0939	1.0692	0.0406	1.1824	0.0003
2146.9	1.1562	0.0211	1.3370	0.0241	1.2396	0.0838	1.0818	0.0414	1.1872	0.0006
2147.4	1.1647	0.0144	1.3381	0.0243	1.2369	0.0722	1.0888	0.0371	1.1913	0.0007
2147.9	1.1724	0.0105	1.3386	0.0246	1.2370	0.0603	1.0964	0.0307	1.1949	0.0008
2148.4	1.1790	0.0076	1.3389	0.0248	1.2377	0.0526	1.1050	0.0241	1.1980	0.0009
2148.9	1.1851	0.0059	1.3390	0.0250	1.2393	0.0432	1.1159	0.0197	1.2009	0.0010
2149.3	1.1885	0.0041	1.3392	0.0253	1.2401	0.0365	1.1202	0.0165	1.2028	0.0010
2149.8	1.1936	0.0035	1.3392	0.0253	1.2441	0.0299	1.1303	0.0151	1.2052	0.0010
2150.3	1.1975	0.0031	1.3393	0.0255	1.2472	0.0228	1.1373	0.0140	1.2073	0.0010
2150.8	1.2006	0.0028	1.3391	0.0257	1.2511	0.0170	1.1433	0.0129	1.2092	0.0010
2151.3	1.2037	0.0019	1.3389	0.0260	1.2565	0.0120	1.1498	0.0114	1.2111	0.0010
2151.7	1.2058	0.0018	1.3388	0.0262	1.2586	0.0094	1.1523	0.0102	1.2122	0.0010
2152.2	1.2083	0.0020	1.3380	0.0262	1.2637	0.0075	1.1581	0.0098	1.2138	0.0011
2152.7	1.2101	0.0020	1.3378	0.0262	1.2675	0.0057	1.1623	0.0087	1.2152	0.0012
2153.2	1.2120	0.0011	1.3372	0.0261	1.2707	0.0051	1.1665	0.0075	1.2165	0.0012
2153.7	1.2140	0.0009	1.3366	0.0257	1.2735	0.0035	1.1703	0.0070	1.2176	0.0013
2154.2	1.2156	0.0014	1.3361	0.0252	1.2765	0.0023	1.1743	0.0059	1.2188	0.0012
2154.6	1.2166	0.0007	1.3359	0.0248	1.2786	0.0010	1.1763	0.0048	1.2195	0.0011
2155.1	1.2183	0.0008	1.3354	0.0242	1.2818	0.0009	1.1806	0.0038	1.2206	0.0012
2156.1	1.2209	0.0008	1.3350	0.0230	1.2861	0.0010	1.1870	0.0037	1.2224	0.0013
2157.1	1.2231	0.0009	1.3347	0.0216	1.2900	0.0015	1.1928	0.0033	1.2242	0.0013
2158.0	1.2246	0.0009	1.3346	0.0201	1.2915	0.0012	1.1968	0.0030	1.2253	0.0014
2159.0	1.2261	0.0007	1.3352	0.0187	1.2959	0.0000	1.2012	0.0026	1.2266	0.0013
2159.9	1.2275	0.0003	1.3357	0.0177	1.2985	0.0019	1.2044	0.0029	1.2275	0.0015
2160.9	1.2291	0.0001	1.3364	0.0165	1.2996	0.0000	1.2083	0.0025	1.2287	0.0016
2161.9	1.2303	0.0006	1.3373	0.0158	1.3019	0.0005	1.2112	0.0028	1.2296	0.0016
2162.8	1.2312	0.0004	1.3383	0.0152	1.3050	0.0000	1.2140	0.0024	1.2303	0.0016
2163.8	1.2322	0.0002	1.3390	0.0150	1.3063	0.0008	1.2165	0.0033	1.2312	0.0017
2164.8	1.2333	0.0002	1.3397	0.0148	1.3074	0.0010	1.2186	0.0030	1.2319	0.0018
2165.7	1.2340	0.0004	1.3403	0.0145	1.3083	0.0000	1.2203	0.0028	1.2323	0.0016
2166.7	1.2352	0.0000	1.3410	0.0147	1.3113	0.0009	1.2229	0.0030	1.2333	0.0018
2167.7	1.2357	0.0005	1.3414	0.0148	1.3124	0.0008	1.2248	0.0033	1.2339	0.0019
2168.6	1.2362	0.0002	1.3418	0.0146	1.3127	0.0021	1.2261	0.0034	1.2342	0.0018
2169.6	1.2371	0.0000	1.3423	0.0147	1.3140	0.0000	1.2276	0.0027	1.2348	0.0017
2172.0	1.2385	0.0000	1.3428	0.0147	1.3177	0.0007	1.2309	0.0037	1.2358	0.0019
2174.4	1.2397	0.0004	1.3433	0.0149	1.3221	0.0000	1.2341	0.0040	1.2367	0.0020
2176.8	1.2408	0.0000	1.3437	0.0149	1.3232	0.0000	1.2361	0.0037	1.2375	0.0019
2179.2	1.2420	0.0001	1.3440	0.0152	1.3254	0.0018	1.2378	0.0046	1.2379	0.0022
2181.6	1.2431	0.0000	1.3441	0.0152	1.3300	0.0008	1.2392	0.0048	1.2385	0.0021
2184.1	1.2442	0.0000	1.3443	0.0155	1.3326	0.0008	1.2417	0.0039	1.2394	0.0019
2186.5	1.2447	0.0000	1.3443	0.0153	1.3331	0.0021	1.2423	0.0043	1.2395	0.0020
2188.9	1.2460	0.0000	1.3445	0.0156	1.3360	0.0012	1.2438	0.0048	1.2400	0.0020
2191.3	1.2467	0.0000	1.3446	0.0152	1.3396	0.0008	1.2450	0.0048	1.2404	0.0020
2193.7	1.2475	0.0000	1.3449	0.0156	1.3412	0.0000	1.2458	0.0045	1.2407	0.0019
2196.1	1.2480	0.0000	1.3447	0.0155	1.3440	0.0000	1.2464	0.0051	1.2409	0.0020
2204.3	1.2506	0.0000	1.3449	0.0154	1.3525	0.0018	1.2486	0.0045	1.2417	0.0017
2211.5	1.2525	0.0000	1.3448	0.0152	1.3592	0.0002	1.2493	0.0045	1.2422	0.0015
2219.7	1.2545	0.0000	1.3446	0.0151	1.3692	0.0000	1.2497	0.0034	1.2425	0.0013
2227.9	1.2562	0.0002	1.3448	0.0148	1.3778	0.0004	1.2514	0.0009	1.2430	0.0009

TABLE 7b - Optical Constants

	Pure CO (n_o = 1.30) ($d = 8.0\times10^{-6}$ cm)		N_2:CO=2:1 (n_o = 1.25) ($d = 5.87\times10^{-5}$ cm)		O_2:CO=20:1 (n_o = 1.25) ($d = 1.15\times10^{-4}$ cm)		CO_2:CO =20:1 (n_o = 1.22) ($d = 1.65\times10^{-6}$ cm)		N_2:H_2O:CO=2:1:1 (n_o = 1.27) ($d = 1.0\times10^{-4}$ cm)	
Freq. (cm^{-1})	***n***	***k***	***n***	***k***	***n***	***k***	***n***	***k***	***n***	***k***
2057.7	1.3371	0.0010	1.2571	0.0007	1.2529	0.0000	1.3035	0.0000	1.2799	0.0001
2065.5	1.3395	0.0017	1.2577	0.0007	1.2532	0.0000	1.3051	0.0001	1.2808	0.0001
2073.2	1.3457	0.0030	1.2585	0.0007	1.2536	0.0000	1.3059	0.0001	1.2819	0.0003
2080.9	1.3538	0.0030	1.2597	0.0009	1.2542	0.0000	1.3074	0.0003	1.2836	0.0002
2088.6	1.3614	0.0111	1.2623	0.0023	1.2558	0.0008	1.3097	0.0000	1.2862	0.0014
2096.3	1.3525	0.0038	1.2604	0.0009	1.2549	0.0000	1.3118	0.0000	1.2858	0.0010
2098.7	1.3594	0.0025	1.2616	0.0009	1.2554	0.0000	1.3126	0.0000	1.2872	0.0011
2101.1	1.3651	0.0035	1.2628	0.0008	1.2558	0.0000	1.3136	0.0000	1.2879	0.0015
2103.6	1.3710	0.0028	1.2638	0.0008	1.2563	0.0000	1.3144	0.0000	1.2887	0.0011
2106.0	1.3766	0.0024	1.2649	0.0012	1.2568	0.0000	1.3153	0.0000	1.2899	0.0004
2108.4	1.3829	0.0019	1.2660	0.0010	1.2574	0.0000	1.3163	0.0000	1.2916	0.0002
2110.8	1.3883	0.0023	1.2673	0.0013	1.2580	0.0001	1.3174	0.0002	1.2937	0.0002
2113.2	1.3956	0.0024	1.2690	0.0017	1.2588	0.0001	1.3185	0.0005	1.2958	0.0003
2115.6	1.4061	0.0015	1.2706	0.0016	1.2598	0.0000	1.3194	0.0010	1.2983	0.0002
2116.6	1.4105	0.0008	1.2716	0.0014	1.2603	0.0000	1.3197	0.0003	1.2993	0.0002
2117.5	1.4154	0.0003	1.2725	0.0017	1.2608	0.0000	1.3205	0.0000	1.3006	0.0001
2118.5	1.4210	0.0000	1.2735	0.0017	1.2614	0.0000	1.3214	0.0005	1.3020	0.0002
2119.5	1.4289	0.0000	1.2745	0.0019	1.2620	0.0000	1.3216	0.0007	1.3033	0.0002
2120.4	1.4346	0.0017	1.2758	0.0017	1.2627	0.0000	1.3221	0.0004	1.3050	0.0002
2121.4	1.4404	0.0008	1.2772	0.0020	1.2635	0.0000	1.3228	0.0005	1.3067	0.0002
2122.4	1.4491	0.0000	1.2786	0.0020	1.2643	0.0000	1.3234	0.0003	1.3085	0.0002
2123.3	1.4582	0.0000	1.2802	0.0022	1.2653	0.0000	1.3243	0.0002	1.3108	0.0003
2124.3	1.4687	0.0002	1.2821	0.0020	1.2666	0.0000	1.3252	0.0002	1.3132	0.0002
2125.2	1.4795	0.0000	1.2843	0.0025	1.2677	0.0000	1.3261	0.0002	1.3158	0.0001
2126.2	1.4921	0.0005	1.2864	0.0026	1.2694	0.0000	1.3271	0.0002	1.3191	0.0002
2127.2	1.5080	0.0000	1.2894	0.0025	1.2713	0.0001	1.3284	0.0004	1.3229	0.0002
2128.1	1.5263	0.0000	1.2926	0.0026	1.2734	0.0000	1.3295	0.0003	1.3269	0.0002
2129.1	1.5485	0.0000	1.2965	0.0029	1.2763	0.0001	1.3311	0.0007	1.3323	0.0003
2130.1	1.5757	0.0000	1.3013	0.0031	1.2796	0.0002	1.3326	0.0009	1.3381	0.0004
2130.6	1.5929	0.0000	1.3040	0.0031	1.2818	0.0003	1.3337	0.0009	1.3420	0.0004
2131.0	1.6093	0.0000	1.3071	0.0034	1.2845	0.0002	1.3344	0.0011	1.3464	0.0007
2131.5	1.6308	0.0000	1.3106	0.0034	1.2877	0.0004	1.3356	0.0015	1.3513	0.0010
2132.0	1.6558	0.0000	1.3145	0.0035	1.2915	0.0004	1.3367	0.0020	1.3571	0.0014
2132.5	1.6848	0.0000	1.3191	0.0037	1.2963	0.0006	1.3379	0.0024	1.3642	0.0020
2133.0	1.7197	0.0013	1.3244	0.0040	1.3009	0.0007	1.3394	0.0030	1.3700	0.0032
2133.4	1.7527	0.0046	1.3306	0.0042	1.3087	0.0012	1.3399	0.0035	1.3793	0.0052
2133.9	1.8025	0.0145	1.3384	0.0049	1.3195	0.0022	1.3417	0.0041	1.3898	0.0085
2134.4	1.8597	0.0354	1.3475	0.0056	1.3348	0.0059	1.3434	0.0051	1.4021	0.0135
2134.9	1.9218	0.0702	1.3588	0.0072	1.3564	0.0165	1.3451	0.0063	1.4163	0.0216
2135.4	1.9869	0.1153	1.3727	0.0103	1.3887	0.0474	1.3470	0.0078	1.4344	0.0337
2135.9	2.0850	0.1559	1.3900	0.0164	1.3788	0.1197	1.3497	0.0096	1.4419	0.0523
2136.3	2.1355	0.2202	1.4099	0.0254	1.3359	0.2133	1.3505	0.0125	1.4586	0.0780
2136.8	2.2776	0.3211	1.4351	0.0376	1.2594	0.2077	1.3525	0.0156	1.4669	0.1126
2137.3	2.4159	0.5410	1.4705	0.0549	1.2300	0.1492	1.3539	0.0194	1.4670	0.1552
2137.8	2.4569	0.9843	1.5190	0.0951	1.2143	0.1276	1.3549	0.0243	1.4626	0.2015
2138.3	2.4082	1.4714	1.5643	0.2098	1.2000	0.1168	1.3558	0.0291	1.4253	0.2489
2138.7	1.8141	2.0591	1.5250	0.4303	1.1882	0.1057	1.3541	0.0385	1.4018	0.2893
2139.2	1.3942	1.9681	1.3614	0.6073	1.1771	0.0889	1.3503	0.0453	1.3492	0.3251
2139.7	0.9789	1.7307	1.1538	0.5721	1.1708	0.0694	1.3435	0.0510	1.2836	0.3435
2140.2	0.8075	1.4179	1.0286	0.4149	1.1694	0.0500	1.3359	0.0529	1.2140	0.3263
2140.7	0.7100	1.1613	0.9820	0.2683	1.1745	0.0348	1.3286	0.0521	1.1812	0.2804
2141.2	0.6186	0.8724	0.9872	0.1690	1.1785	0.0219	1.3254	0.0464	1.1287	0.2226
2141.6	0.5781	0.7956	1.0087	0.1061	1.1842	0.0122	1.3200	0.0497	1.1267	0.1680
2142.1	0.5384	0.6529	1.0328	0.0635	1.1919	0.0060	1.3179	0.0455	1.1307	0.1224
2142.6	0.5228	0.5934	1.0597	0.0306	1.1988	0.0027	1.3149	0.0436	1.1438	0.0891

TABLE 7b - Optical Constants (*continued*)

	Pure CO		N_2:CO=2:1		O_2:CO=20:1		CO_2:CO =20:1		N_2:H_2O:CO=2:1:1	
Freq. (cm^{-1})	***n***	***k***	***n***	***k***	***n***	***k***	***n***	***k***	***n***	***k***
2143.1	0.5391	0.4825	1.0868	0.0085	1.2048	0.0008	1.3121	0.0417	1.1608	0.0664
2143.6	0.5635	0.3066	1.1116	0.0016	1.2096	0.0000	1.3089	0.0398	1.1814	0.0532
2144.1	0.6203	0.1642	1.1302	0.0000	1.2130	0.0000	1.3072	0.0342	1.1915	0.0464
2144.5	0.6681	0.1050	1.1443	0.0000	1.2163	0.0000	1.3061	0.0352	1.2099	0.0458
2145.0	0.7553	0.0725	1.1552	0.0000	1.2191	0.0000	1.3055	0.0314	1.2225	0.0486
2145.5	0.8156	0.0536	1.1641	0.0000	1.2214	0.0000	1.3047	0.0290	1.2321	0.0542
2146.0	0.8642	0.0457	1.1714	0.0000	1.2233	0.0000	1.3038	0.0271	1.2397	0.0619
2146.5	0.9056	0.0426	1.1775	0.0000	1.2247	0.0000	1.3037	0.0237	1.2413	0.0703
2146.9	0.9224	0.0405	1.1827	0.0000	1.2262	0.0000	1.3037	0.0232	1.2421	0.0794
2147.4	0.9512	0.0350	1.1871	0.0000	1.2276	0.0000	1.3036	0.0203	1.2385	0.0877
2147.9	0.9740	0.0294	1.1909	0.0000	1.2287	0.0000	1.3039	0.0187	1.2325	0.0947
2148.4	1.0148	0.0259	1.1944	0.0000	1.2298	0.0000	1.3041	0.0173	1.2238	0.0993
2148.9	1.0133	0.0232	1.1975	0.0000	1.2307	0.0000	1.3041	0.0158	1.2169	0.1014
2149.4	1.0315	0.0216	1.2002	0.0000	1.2314	0.0000	1.3046	0.0134	1.2018	0.0994
2149.8	1.0403	0.0196	1.2025	0.0000	1.2322	0.0000	1.3051	0.0123	1.1971	0.0953
2150.3	1.0560	0.0196	1.2047	0.0000	1.2330	0.0000	1.3060	0.0106	1.1879	0.0882
2150.8	1.0676	0.0203	1.2068	0.0000	1.2337	0.0000	1.3068	0.0097	1.1806	0.0789
2151.3	1.0772	0.0203	1.2088	0.0000	1.2343	0.0000	1.3073	0.0089	1.1771	0.0690
2151.8	1.0875	0.0194	1.2106	0.0000	1.2347	0.0000	1.3080	0.0076	1.1736	0.0577
2152.2	1.0909	0.0180	1.2121	0.0000	1.2353	0.0000	1.3084	0.0066	1.1746	0.0478
2152.7	1.1007	0.0165	1.2135	0.0000	1.2358	0.0000	1.3093	0.0054	1.1759	0.0382
2153.2	1.1080	0.0159	1.2148	0.0000	1.2363	0.0000	1.3102	0.0042	1.1786	0.0299
2153.7	1.1151	0.0141	1.2161	0.0000	1.2367	0.0000	1.3112	0.0032	1.1822	0.0227
2154.2	1.1224	0.0127	1.2173	0.0000	1.2372	0.0000	1.3125	0.0022	1.1876	0.0171
2154.7	1.1302	0.0133	1.2183	0.0000	1.2375	0.0001	1.3139	0.0017	1.1890	0.0122
2155.1	1.1324	0.0133	1.2194	0.0000	1.2379	0.0000	1.3146	0.0013	1.1953	0.0089
2156.1	1.1440	0.0119	1.2213	0.0000	1.2386	0.0001	1.3170	0.0009	1.2042	0.0046
2157.1	1.1536	0.0113	1.2229	0.0000	1.2392	0.0002	1.3185	0.0011	1.2117	0.0026
2158.0	1.1607	0.0102	1.2244	0.0002	1.2397	0.0002	1.3197	0.0002	1.2170	0.0018
2159.0	1.1700	0.0114	1.2256	0.0001	1.2402	0.0002	1.3217	0.0003	1.2218	0.0015
2160.0	1.1759	0.0122	1.2268	0.0002	1.2405	0.0002	1.3230	0.0003	1.2251	0.0015
2160.9	1.1800	0.0102	1.2278	0.0002	1.2410	0.0003	1.3241	0.0004	1.2284	0.0015
2161.9	1.1866	0.0085	1.2289	0.0001	1.2413	0.0003	1.3252	0.0003	1.2311	0.0015
2162.9	1.1939	0.0099	1.2300	0.0002	1.2416	0.0003	1.3263	0.0000	1.2331	0.0015
2163.8	1.1955	0.0112	1.2308	0.0004	1.2419	0.0004	1.3276	0.0002	1.2352	0.0015
2164.8	1.1999	0.0083	1.2316	0.0004	1.2421	0.0003	1.3284	0.0005	1.2371	0.0015
2165.7	1.2044	0.0090	1.2322	0.0004	1.2424	0.0003	1.3293	0.0001	1.2384	0.0015
2166.7	1.2074	0.0112	1.2331	0.0005	1.2426	0.0003	1.3305	0.0004	1.2401	0.0015
2167.7	1.2099	0.0080	1.2336	0.0006	1.2428	0.0003	1.3313	0.0004	1.2415	0.0015
2168.6	1.2145	0.0077	1.2341	0.0006	1.2430	0.0003	1.3322	0.0004	1.2425	0.0015
2169.6	1.2183	0.0095	1.2348	0.0004	1.2432	0.0003	1.3329	0.0005	1.2435	0.0016
2172.0	1.2232	0.0094	1.2360	0.0008	1.2437	0.0002	1.3355	0.0003	1.2459	0.0015
2174.4	1.2290	0.0094	1.2370	0.0010	1.2441	0.0002	1.3374	0.0004	1.2478	0.0016
2176.8	1.2352	0.0115	1.2380	0.0008	1.2444	0.0002	1.3396	0.0003	1.2494	0.0016
2179.2	1.2363	0.0097	1.2384	0.0014	1.2447	0.0002	1.3420	0.0000	1.2506	0.0015
2181.7	1.2416	0.0116	1.2392	0.0013	1.2450	0.0001	1.3445	0.0003	1.2518	0.0016
2184.1	1.2449	0.0114	1.2396	0.0014	1.2453	0.0001	1.3467	0.0004	1.2531	0.0016
2186.5	1.2461	0.0118	1.2399	0.0014	1.2454	0.0000	1.3492	0.0000	1.2539	0.0015
2188.9	1.2486	0.0131	1.2405	0.0015	1.2457	0.0000	1.3519	0.0002	1.2547	0.0015
2191.3	1.2472	0.0120	1.2410	0.0016	1.2459	0.0001	1.3543	0.0000	1.2554	0.0014
2193.7	1.2532	0.0068	1.2412	0.0016	1.2461	0.0001	1.3572	0.0001	1.2562	0.0014
2196.1	1.2563	0.0122	1.2414	0.0018	1.2463	0.0001	1.3599	0.0003	1.2567	0.0015
2204.3	1.2592	0.0151	1.2421	0.0018	1.2467	0.0000	1.3691	0.0000	1.2584	0.0013
2211.5	1.2573	0.0144	1.2422	0.0014	1.2471	0.0000	1.3790	0.0002	1.2594	0.0013
2219.7	1.2587	0.0101	1.2423	0.0012	1.2474	0.0000	1.3912	0.0005	1.2603	0.0012
2227.9	1.2581	0.0072	1.2428	0.0000	1.2476	0.0001	1.4057	0.0000	1.2611	0.0010
2236.1	1.2649	0.0008	1.2439	0.0000	1.2478	0.0001	1.4212	0.0004	1.2617	0.0008

TABLE 8 - Column Densities of Solid CO in Non-Polar Interstellar Ices and the Percent of Cosmic Nitrogen and Oxygen in the form of Frozen N_2 and O_2 in the Quiescent Regions of Dense Molecular Clouds

Object	N(H) ($\times 10^{22}$ cm^{-2})	$N(CO)_{non\text{-}polar}$ ($\times 10^{17}$ cm^{-2})	%N in Solid N_2	%O in Solid O_2
Taurus[a]	(b)	(a)		
Elias 1 (em)	1.7	0.5	9.7	6
Elias 3 (bkgd)	1.6	1.7	37	23
Elias 13 (bkgd)	2.0	0.9	15	9.5
Elias 16 (bkgd)	4.2	5.6	43	27
Elias 18 (em)	3.5	1.6	15	9.5
Tamura 8 (bkgd)	3.5	4.7	43	27
Serpens[c]	(b)			
CK 1 (bkgd?)	2.9	6.5[d]	73	46
CK 2 (bkgd)	8.7	10	40	25
CK 3 (bkgd?)	1.8	0.87	16	10
SVS 4 (bkgd?)	4.8	2.3	16	10
SVS 9 (bkgd?)	2.8	<2.6	30	19
Miscellaneous[e]	(e)	(e)		
NGC 7538 IRS9 (em)	16	6.4	13	8.5
L1551 IRS 5 (em)	2.3	2.3	33	21
W33A (em)	2.8	1.1	1.3	1
AFGL 961 (em)	7.4	1.5	6.7	4
NGC 2024 IRS2 (em)	6.0	1.2	6.7	4

(em) $\Rightarrow$ object is embedded in the molecular cloud; (bkgd) $\Rightarrow$ object is behind the molecular cloud.

(a) From Chiar et al. (1995)

(b) Calculated from A_V as described in §5.1

(c) From Chiar et al. (1994)

(d) Assumes all CO is in a non-polar ice; see Eiroa & Hodapp (1989)

(e) From Tielens et al. (1991)

FIGURE CAPTIONS

Figure 1. The concentration dependence of the CO band in N_2:CO ices at 12 K. All spectra are plotted on the scale indicated by the bar in the lower right side of the figure. The spectra are offset vertically from each other for clarity.

Figure 2. The temperature dependence of the CO band in a N_2:CO = 1:20 ice. All spectra are plotted on the scale indicated by the bar in the lower right side of the figure. The spectra are offset vertically from each other for clarity.

Figure 3. The concentration dependence of the CO band in N_2:H_2O:CO ices at 12 K. All spectra are plotted on the scale indicated by the bar in the lower left side of the figure. The spectra are offset vertically from each other for clarity. The extra feature peaking near 2148 cm^{-1} in several mixtures is induced by the presence of H_2O.

Figure 4. The CO band produced by several O_2:CO and N_2:O_2:CO ices at 12 K. All spectra are plotted on the scale indicated by the bar in the lower right side of the figure. The spectra are offset vertically from each other for clarity.

Figure 5. The CO band produced by several CO_2:CO and N_2:CO_2:CO ices at 12 K. All spectra are plotted on the scale indicated by the bar in the lower left side of the figure. The spectra are offset vertically from each other for clarity.

Figure 6. The CO band produced by several N_2:O_2:CO_2:CO ices at 12 K. All spectra are plotted on the scale indicated by the bar in the lower left side of the figure. The spectra are offset vertically from each other for clarity.

Figure 7. The spectrum of an N_2:O_2:CO = 1:1:1 ice at 12 K before (upper trace) and after (lower trace) 3 hours of UV photolysis.

Figure 8. The new bands due to photoproducts made when an N_2:H_2O:CO = 2:1:1 ice at 12 K is UV irradiated for 3 hours. In all cases, the upper traces is of the ice prior to irradiation and the lower trace is of the ice after irradiation.

Figure 9. The new bands due to photoproducts made when an N_2:O_2:CO = 1:1:1 ice at 12 K is UV irradiated for 3 hours. In all cases, the upper traces is of the ice prior to irradiation and the lower trace is of the ice after irradiation.

Figure 10. The N_2 stretching bands produced by N_2:CO = 1:100 (upper trace) and N_2:H_2O:CO = 1:1:1 (lower trace) ices at 12 K.

Figure 11. The O_2 stretching band produced by an N_2:O_2:CO = 1:1:1 ice at 12 K before (upper trace) and after (lower trace) UV irradiation. Band strength enhancement is presumably due to the introduction of additional irregularities into the ice structure by photolysis.

Figure 12. A comparison between the solid CO ice in the spectrum of NGC 7538 IRS9 (thick solid line; taken from Tielens et al. 1991) and the features produced by the ices H_2O:CO=20:1, N_2:O_2:CO=1:5:1, N_2:H_2O:CO=5:1:5, and N_2:CO_2:CO=1:5:1 at 12 K(various thin lines). This demonstrates that (i) H_2O-rich ices can reproduce the 2135 cm^{-1} component of the interstellar feature, (ii) the features produced by non-polar ices dominated by N_2 and O_2 are too narrow and fall ~1 cm^{-1} to the red, and (iii) the added presence of CO_2 produces dramatic increases in the width and frequency of the band.

Figure 13. A comparison between the solid CO ice feature in the spectra of NGC 7538 IRS9, AFGL 961, Elias 16, and Elias #18 (thick solid lines; taken from Tielens et al. 1991) and the features produced by coadding bands from two ice analogs (dotted lines). Fits were obtained by coadding differing amounts of absorption due to CO in a non-polar ice and CO in a polar (H_2O:CO=20:1) ice. (a) The fit provided to the spectrum of NGC 7538 IRS9 by a combination of CO_2:CO=20:1 (67%) and H_2O:CO=20:1 (33%) ices. This fit requires too much cosmic C be in the form of CO_2, fails to match the interstellar band position, and does

not account for the high frequency wing of the interstellar feature. (b) The fit provided to the spectra of NGC 7538 IRS9 and Elias #16 by a combination of N_2:O_2:CO_2:CO=1:5:$^1/_2$:1 (67%) and H_2O:CO=20:1 (33%) ices. (c) The fit provided to the spectra of AFGL 961 and Elias #18 by a combination of N_2:O_2:CO_2:CO=1:5:$^1/_2$:1 (50%) and H_2O:CO=20:1 (50%) ices. Coadds with the N_2:O_2:CO_2:CO=1:5:$^1/_2$:1 ice produce a much better fit. Higher proportions of the polar, H_2O-rich ice component are required for the embedded objects AFGL 961 and Elias 18, suggesting that these lines of sight sample the vicinities of newly forming stars where the interstellar ices may be partially 'distilled' of their more volatile, non-polar components.

Figure 1

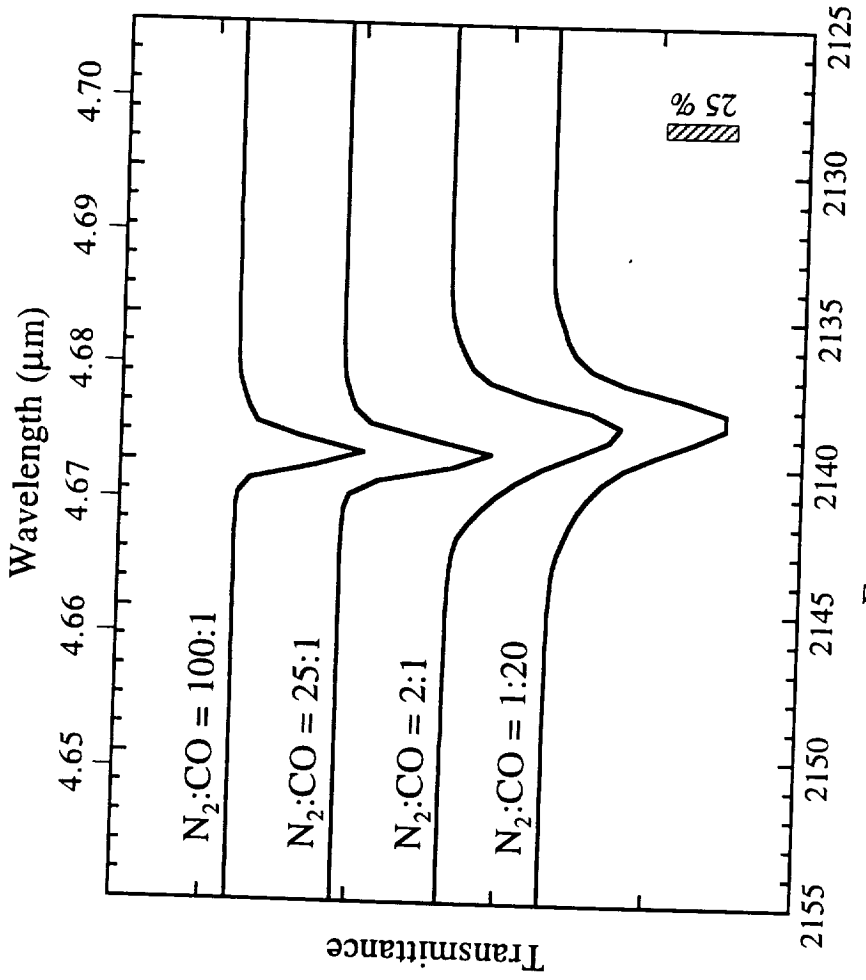
Wavelength (μm)
4.65
4.66
4.67
4.68
4.69
4.70
Frequency (cm-1)
2155
2150
2145
2140
2135
2130
2125
Transmittance
N2:CO = 100:1
N2:CO = 25:1
N2:CO = 2:1
N2:CO = 1:20
25 %

Figure 2

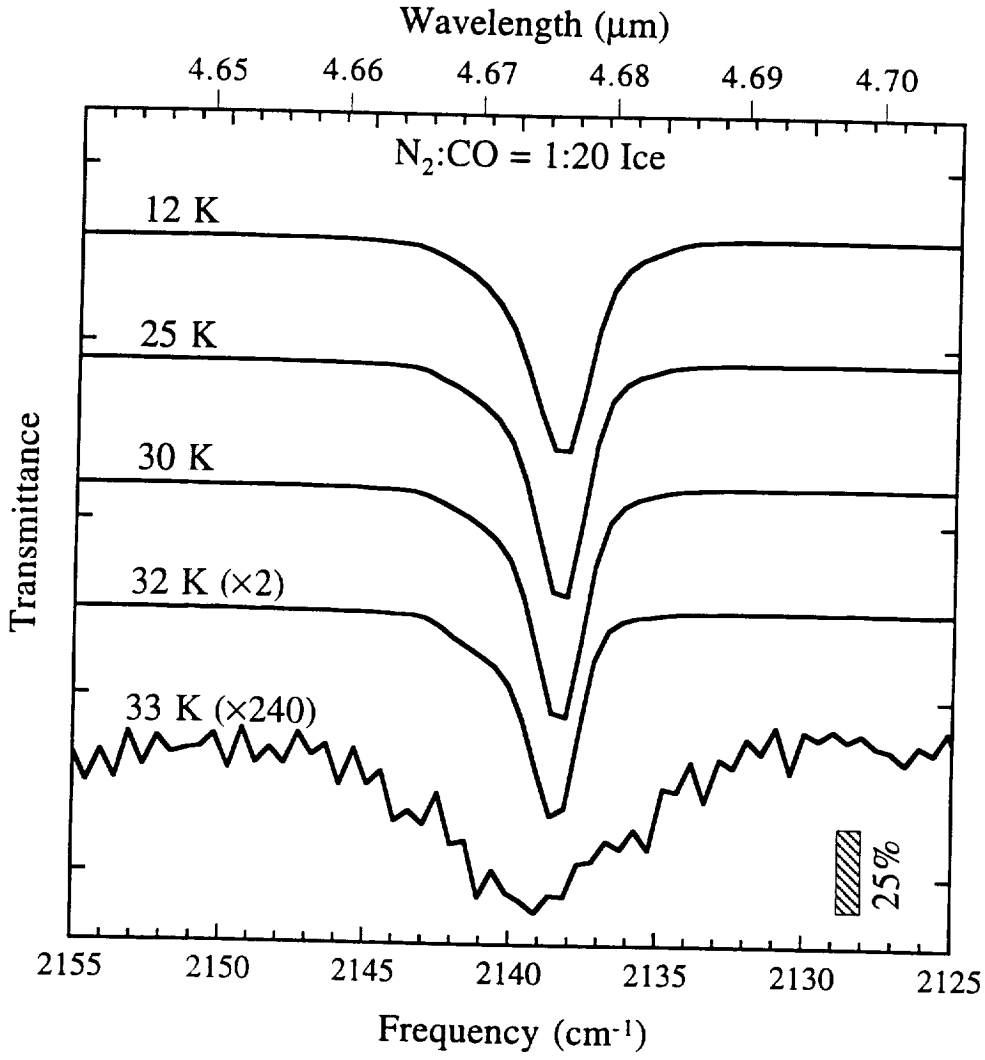
Wavelength (μm)
4.65
4.66
4.67
4.68
4.69
4.70
N2:CO = 1:20 Ice
12 K
25 K
30 K
32 K (×2)
33 K (×240)
25%
Transmittance
2155
2150
2145
2140
2135
2130
2125
Frequency (cm-1)

Figure 3

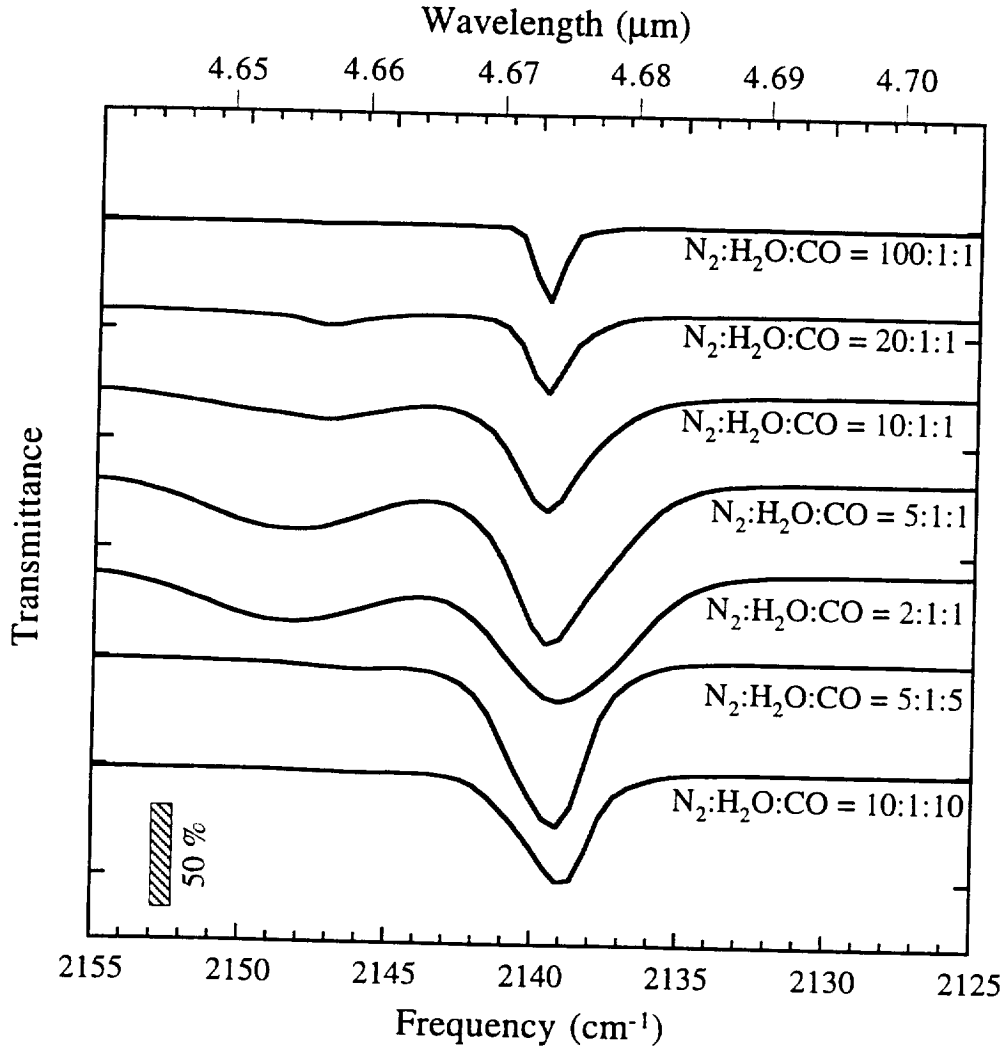
Wavelength (μm)
4.65
4.66
4.67
4.68
4.69
4.70
N_2:H_2O:CO = 100:1:1
N_2:H_2O:CO = 20:1:1
N_2:H_2O:CO = 10:1:1
N_2:H_2O:CO = 5:1:1
N_2:H_2O:CO = 2:1:1
N_2:H_2O:CO = 5:1:5
N_2:H_2O:CO = 10:1:10
50 %
Transmittance
2155
2150
2145
2140
2135
2130
2125
Frequency (cm^{-1})

Figure 4

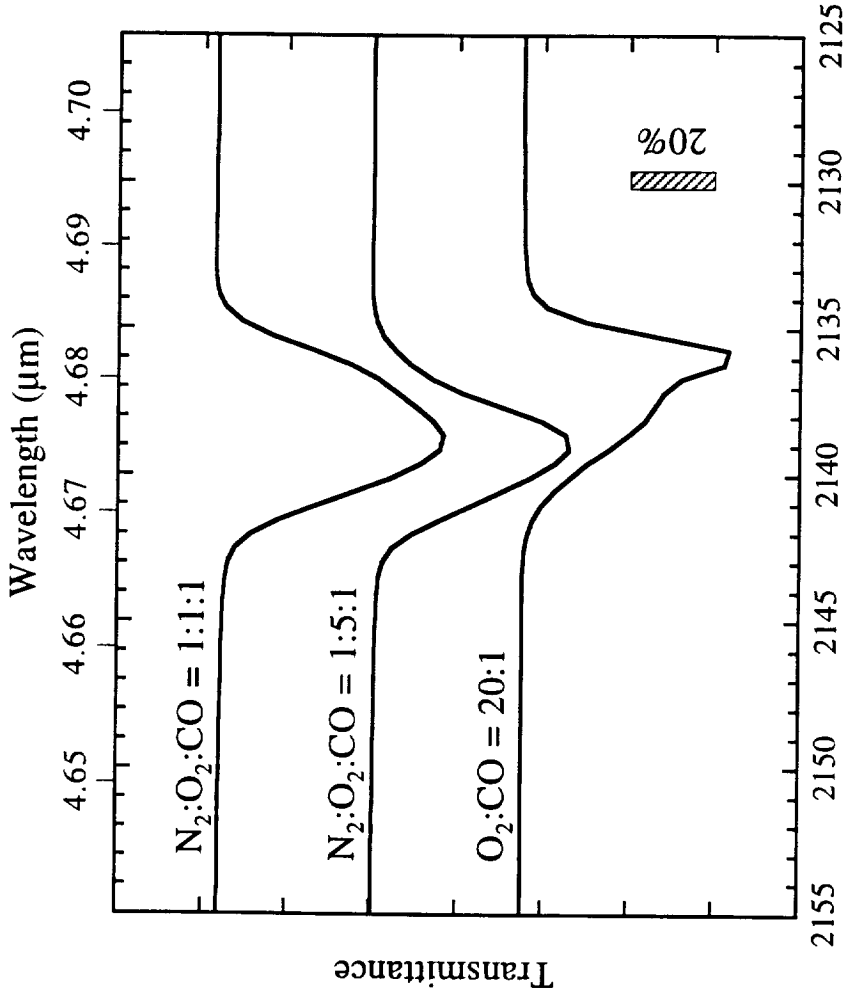
Wavelength (μm)
4.65
4.66
4.67
4.68
4.69
4.70
Frequency (cm-1)
2155
2150
2145
2140
2135
2130
2125
Transmittance
N2:O2:CO = 1:1:1
N2:O2:CO = 1:5:1
O2:CO = 20:1
20%

Figure 5

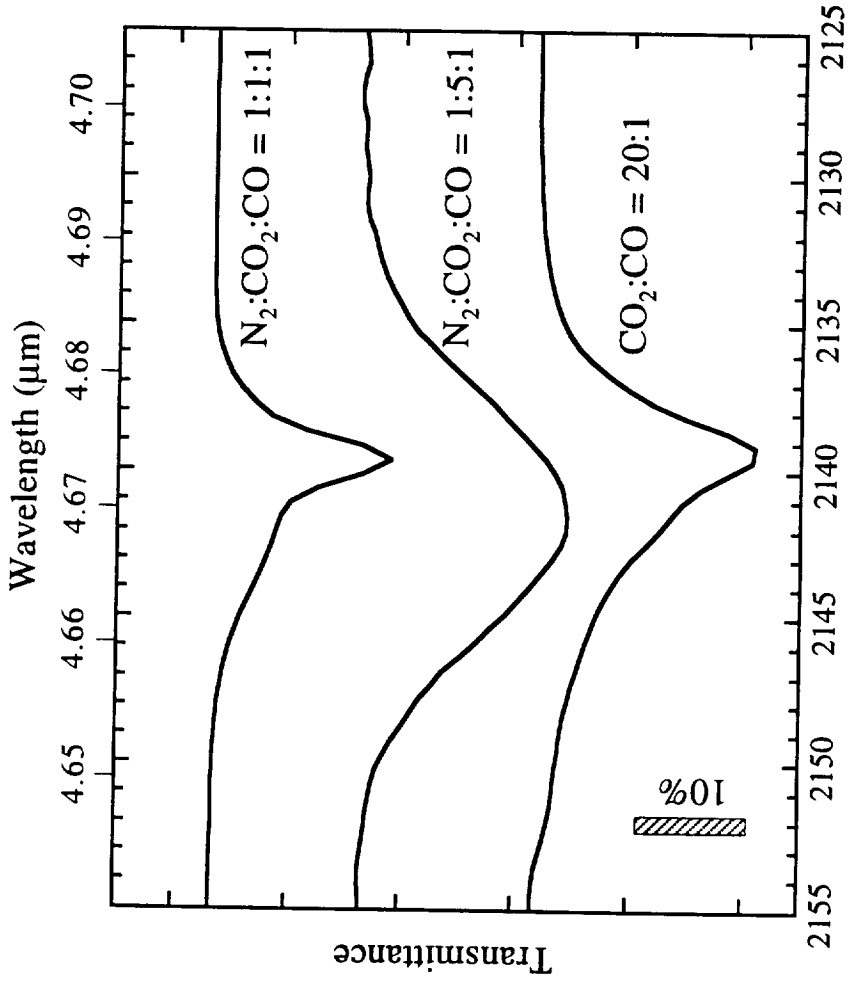
Wavelength (μm)
4.65
4.66
4.67
4.68
4.69
4.70
Frequency (cm-1)
2155
2150
2145
2140
2135
2130
2125
Transmittance
N2:CO2:CO = 1:1:1
N2:CO2:CO = 1:5:1
CO2:CO = 20:1
10%

Figure 6

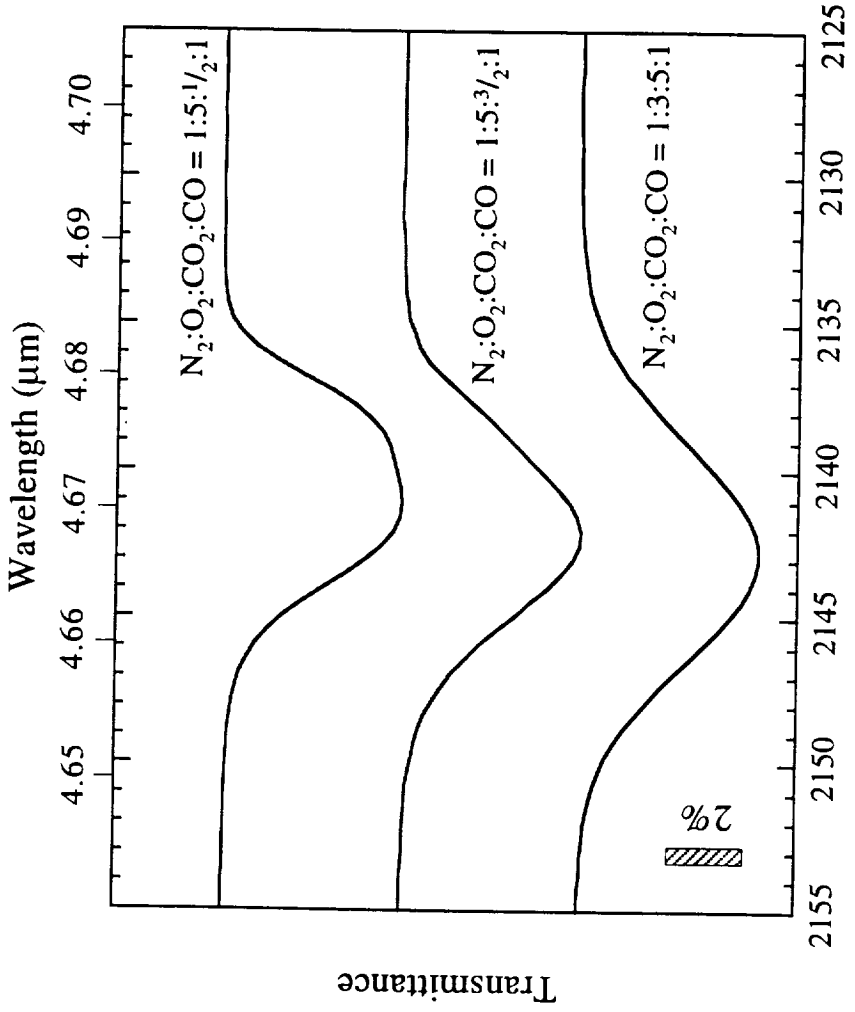
Wavelength (μm)
4.65
4.66
4.67
4.68
4.69
4.70
Frequency (cm-1)
2155
2150
2145
2140
2135
2130
2125
Transmittance
2%
N2:O2:CO2:CO = 1:5:1/2:1
N2:O2:CO2:CO = 1:5:3/2:1
N2:O2:CO2:CO = 1:3:5:1

Figure 7

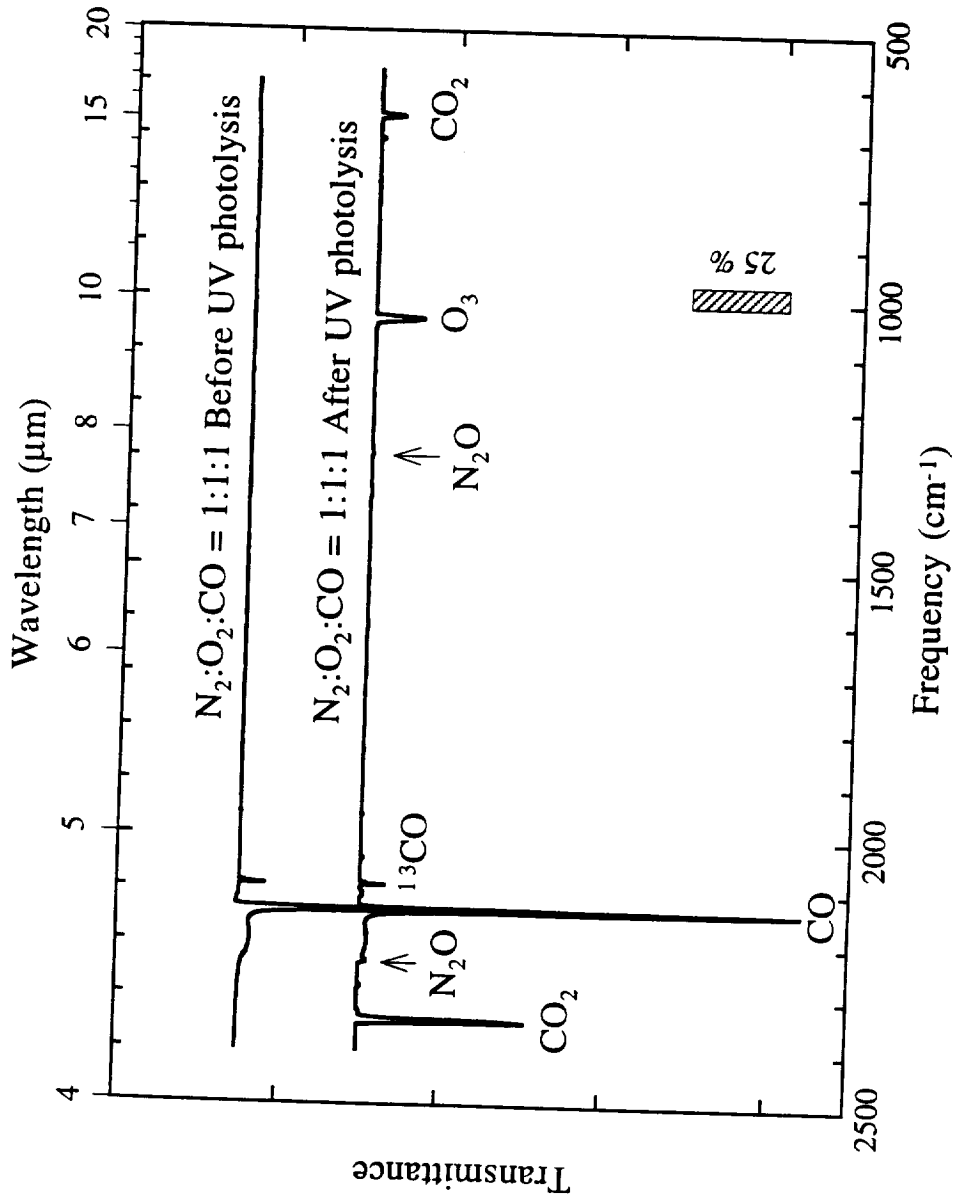
Wavelength (μm)
4
5
6
7
8
10
15
20
2500
2000
1500
1000
500
Frequency (cm-1)
Transmittance
N2:O2:CO = 1:1:1 Before UV photolysis
N2:O2:CO = 1:1:1 After UV photolysis
CO2
N2O
13CO
CO
CO2
N2O
O3
25 %

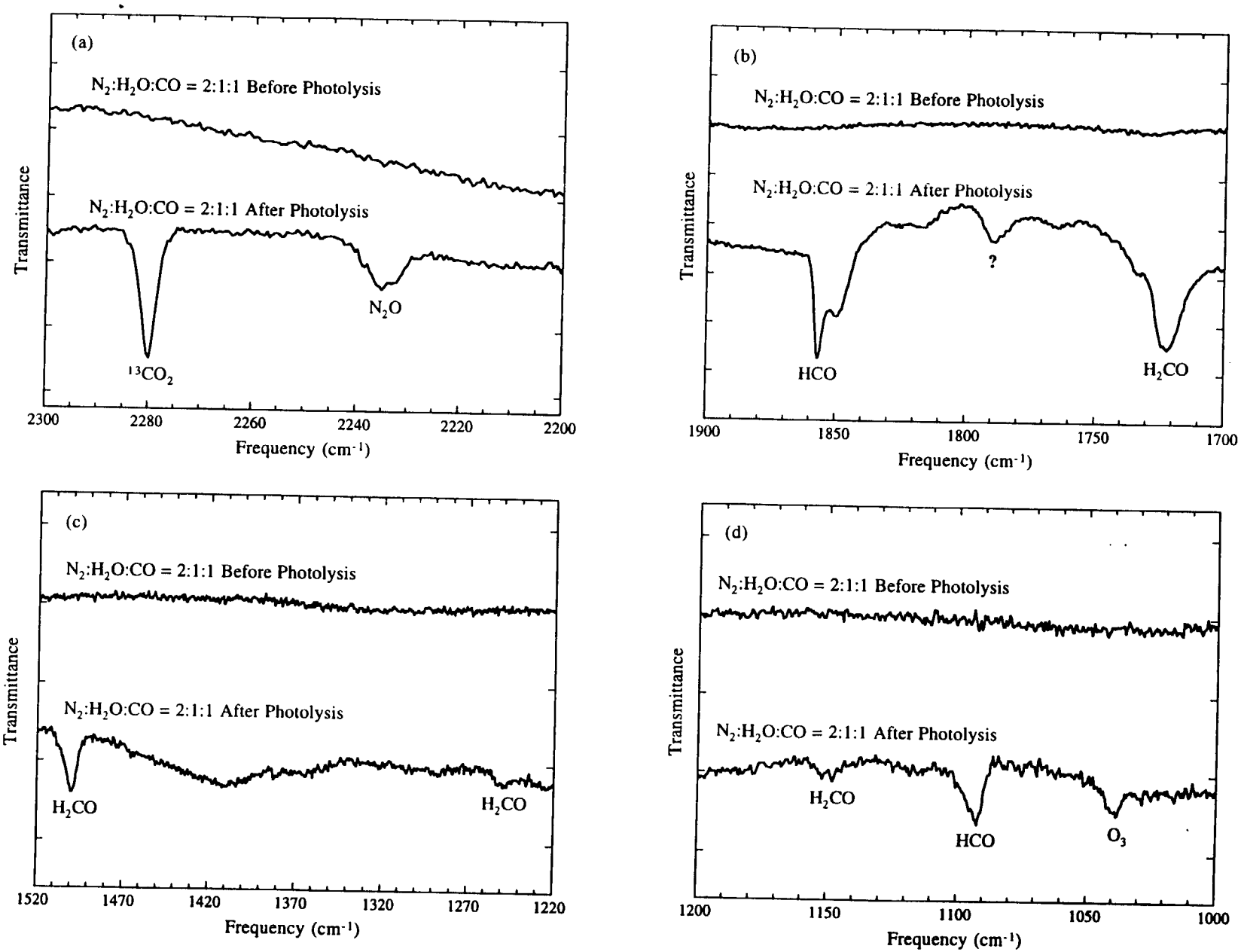
(a)
N_2:H_2O:CO = 2:1:1 Before Photolysis
N_2:H_2O:CO = 2:1:1 After Photolysis
$^{13}CO_2$
N_2O
Transmittance
2300
2280
2260
2240
2220
2200
Frequency (cm^{-1})
(b)
N_2:H_2O:CO = 2:1:1 Before Photolysis
N_2:H_2O:CO = 2:1:1 After Photolysis
?
HCO
H_2CO
Transmittance
1900
1850
1800
1750
1700
Frequency (cm^{-1})
(c)
N_2:H_2O:CO = 2:1:1 Before Photolysis
N_2:H_2O:CO = 2:1:1 After Photolysis
H_2CO
H_2CO
Transmittance
1520
1470
1420
1370
1320
1270
1220
Frequency (cm^{-1})
(d)
N_2:H_2O:CO = 2:1:1 Before Photolysis
N_2:H_2O:CO = 2:1:1 After Photolysis
H_2CO
HCO
O_3
Transmittance
1200
1150
1100
1050
1000
Frequency (cm^{-1})

Figure 8

Figure 9

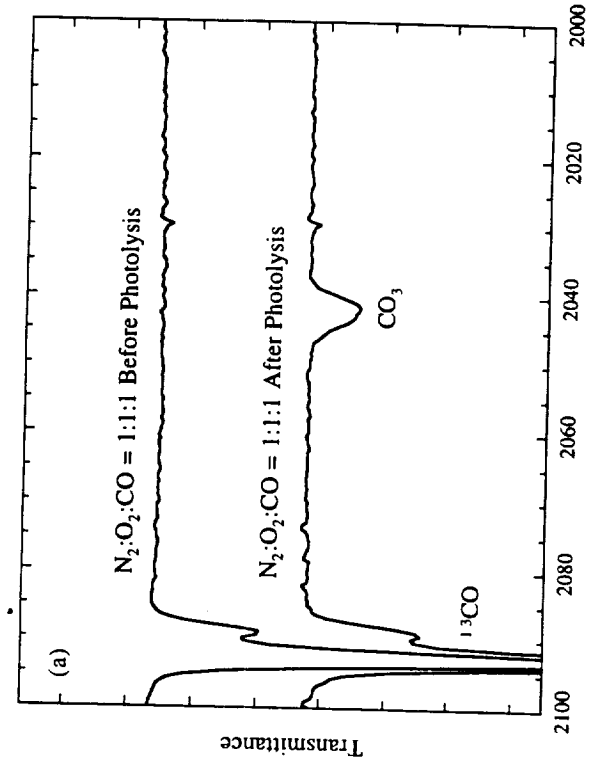
(a)
N_2:O_2:CO = 1:1:1 Before Photolysis
N_2:O_2:CO = 1:1:1 After Photolysis
CO_3
^{13}CO
Transmittance
2100
2080
2060
2040
2020
2000
Frequency (cm^{-1})

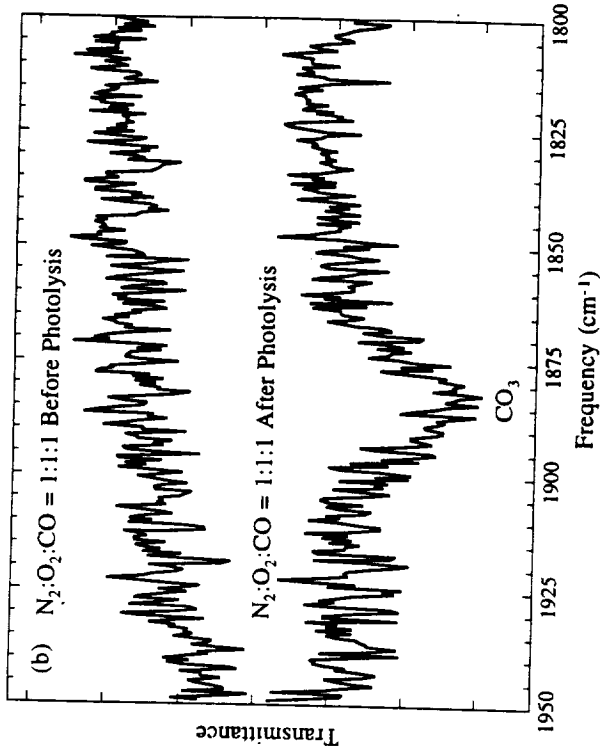
(b)
N_2:O_2:CO = 1:1:1 Before Photolysis
N_2:O_2:CO = 1:1:1 After Photolysis
CO_3
Transmittance
1950
1925
1900
1875
1850
1825
1800
Frequency (cm^{-1})

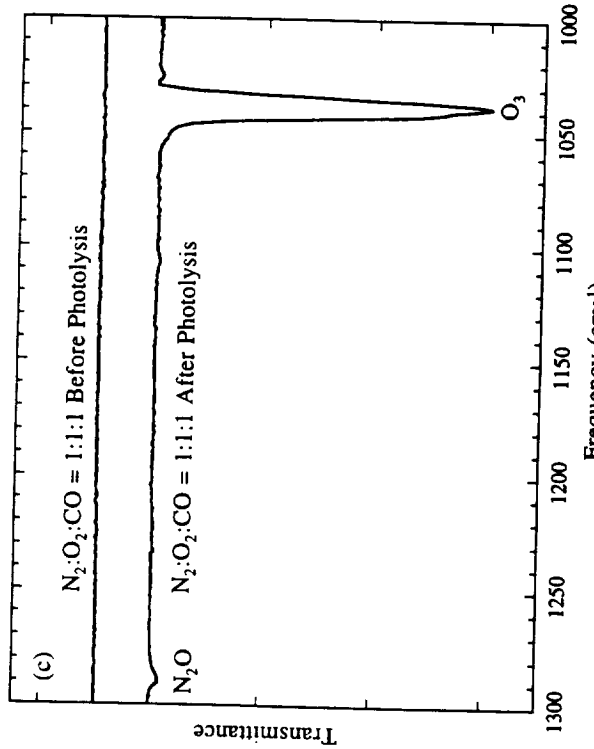
(c)
N_2:O_2:CO = 1:1:1 Before Photolysis
N_2:O_2:CO = 1:1:1 After Photolysis
N_2O
O_3
Transmittance
1300
1250
1200
1150
1100
1050
1000
Frequency (cm^{-1})

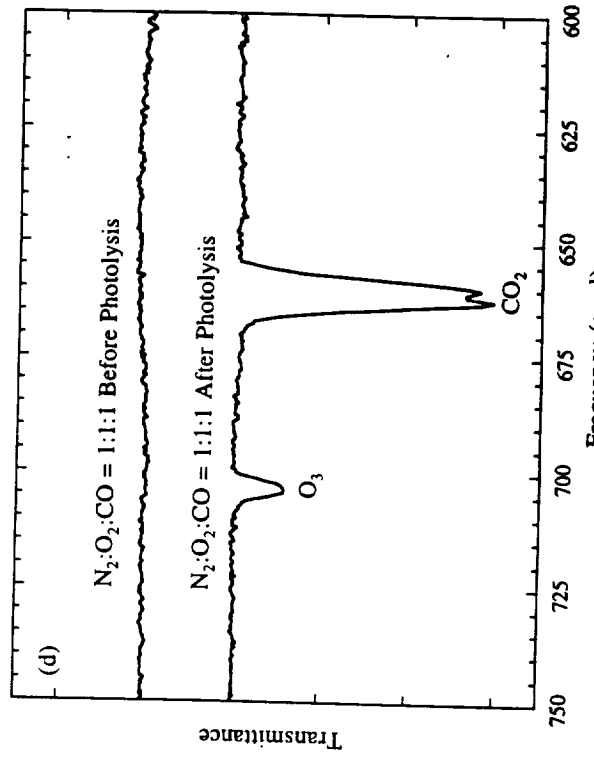
(d)
N_2:O_2:CO = 1:1:1 Before Photolysis
N_2:O_2:CO = 1:1:1 After Photolysis
O_3
CO_2
Transmittance
750
725
700
675
650
625
600
Frequency (cm^{-1})

Figure 10

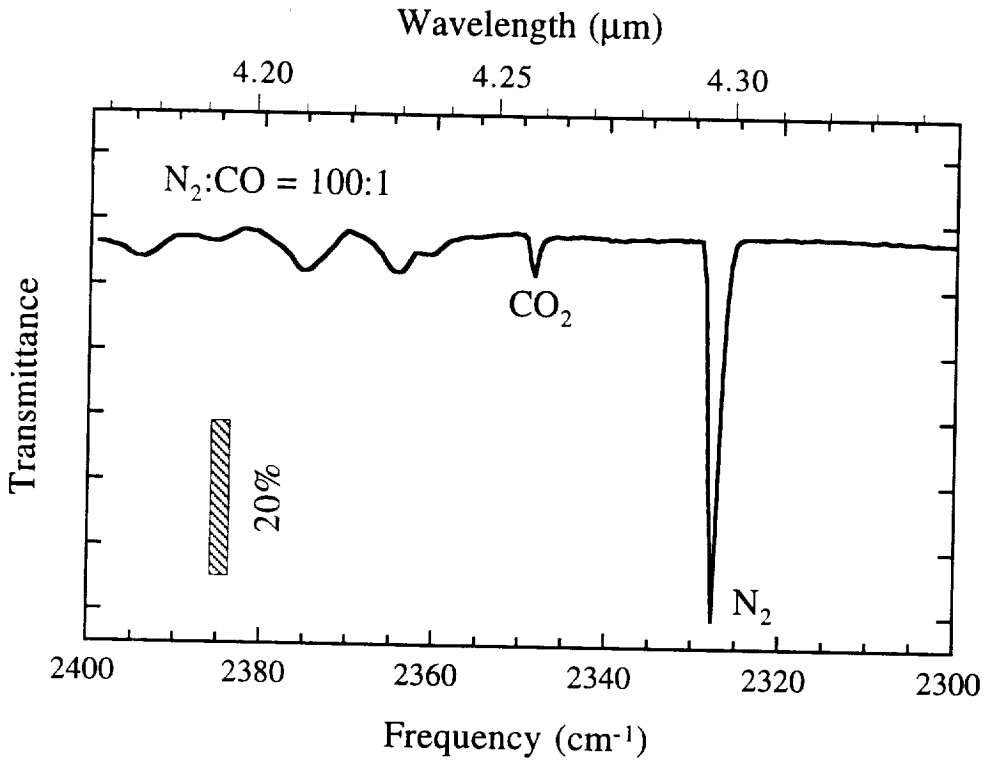
Wavelength (μm)
4.20
4.25
4.30
N2:CO = 100:1
CO2
20%
N2
Transmittance
2400
2380
2360
2340
2320
2300
Frequency (cm-1)

Figure 11

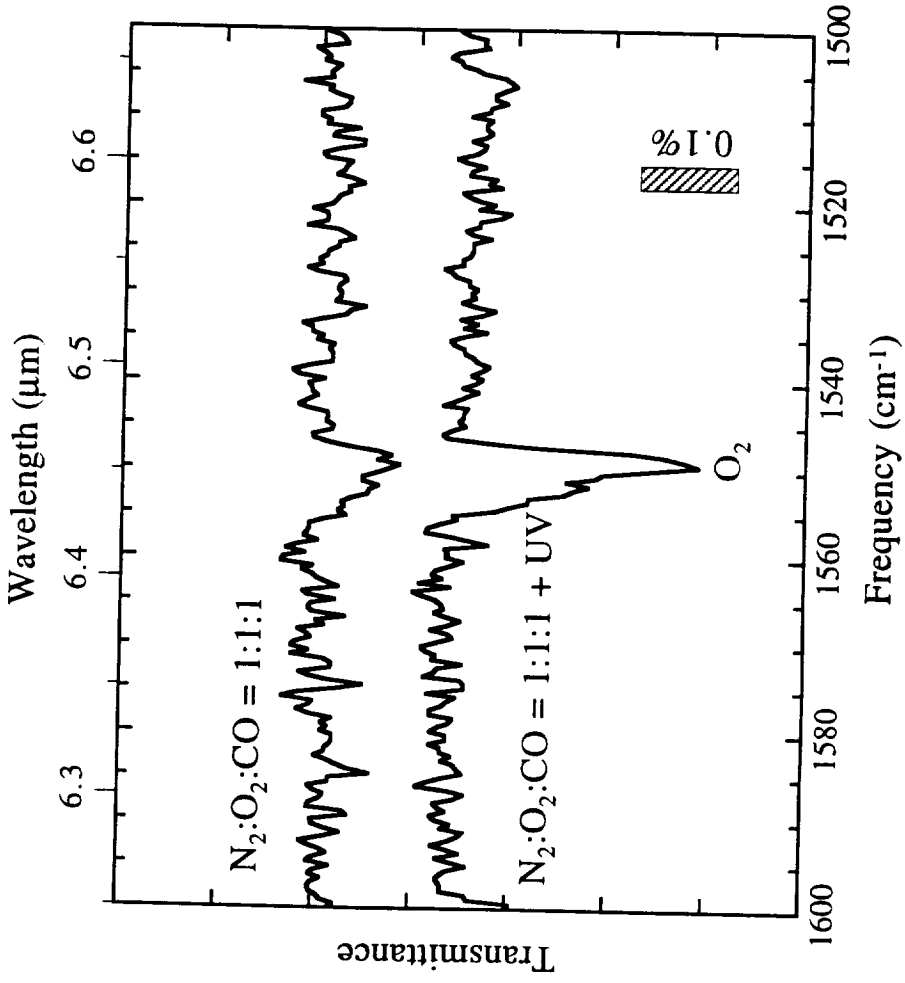
Wavelength (μm)
6.3
6.4
6.5
6.6
Frequency (cm-1)
1600
1580
1560
1540
1520
1500
Transmittance
N2:O2:CO = 1:1:1
N2:O2:CO = 1:1:1 + UV
O2
0.1%

Figure 12

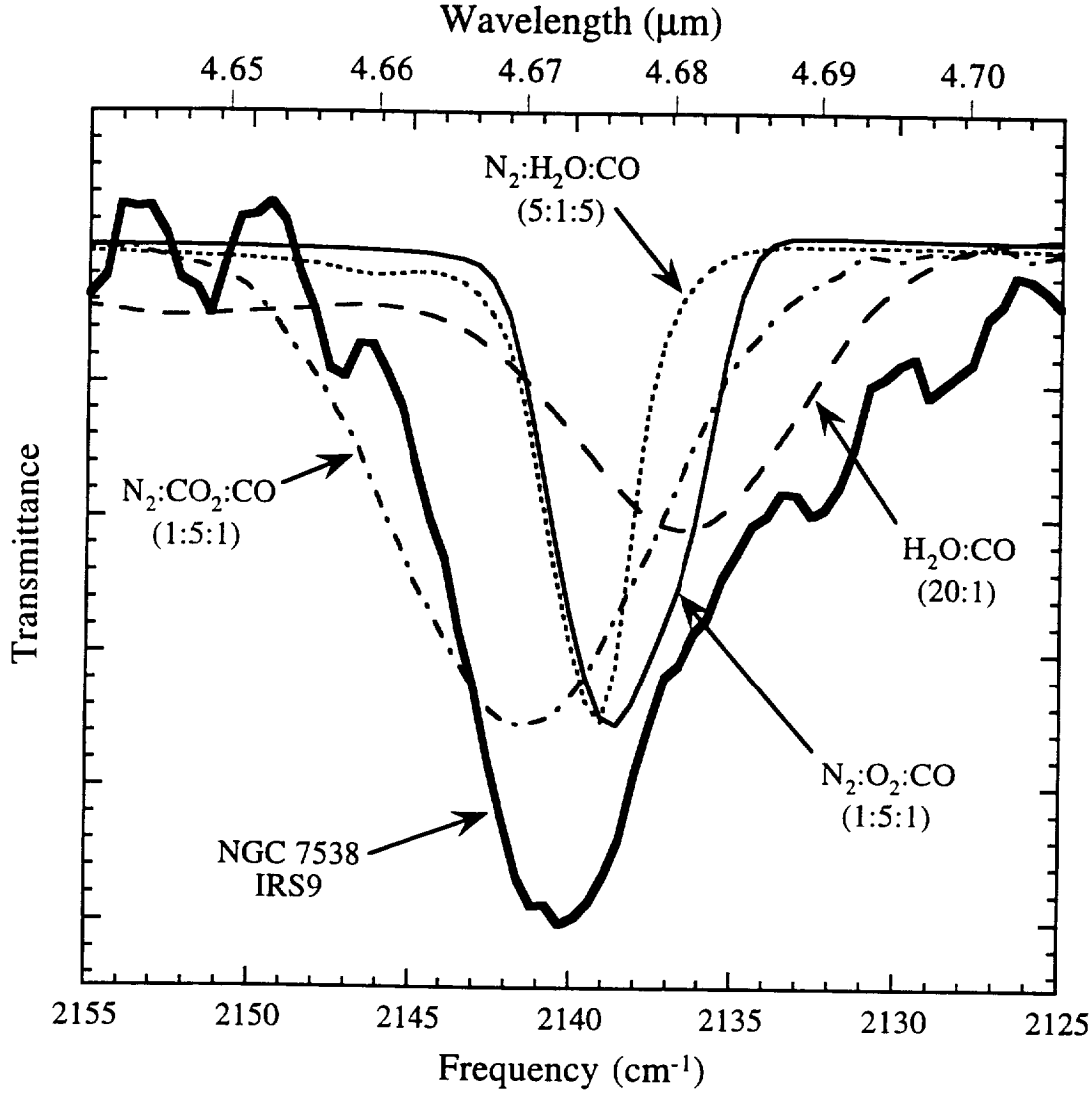
Wavelength (μm)
4.65
4.66
4.67
4.68
4.69
4.70
N_2:H_2O:CO
(5:1:5)
N_2:CO_2:CO
(1:5:1)
H_2O:CO
(20:1)
N_2:O_2:CO
(1:5:1)
NGC 7538
IRS9
Transmittance
2155
2150
2145
2140
2135
2130
2125
Frequency (cm^{-1})

Figure 13

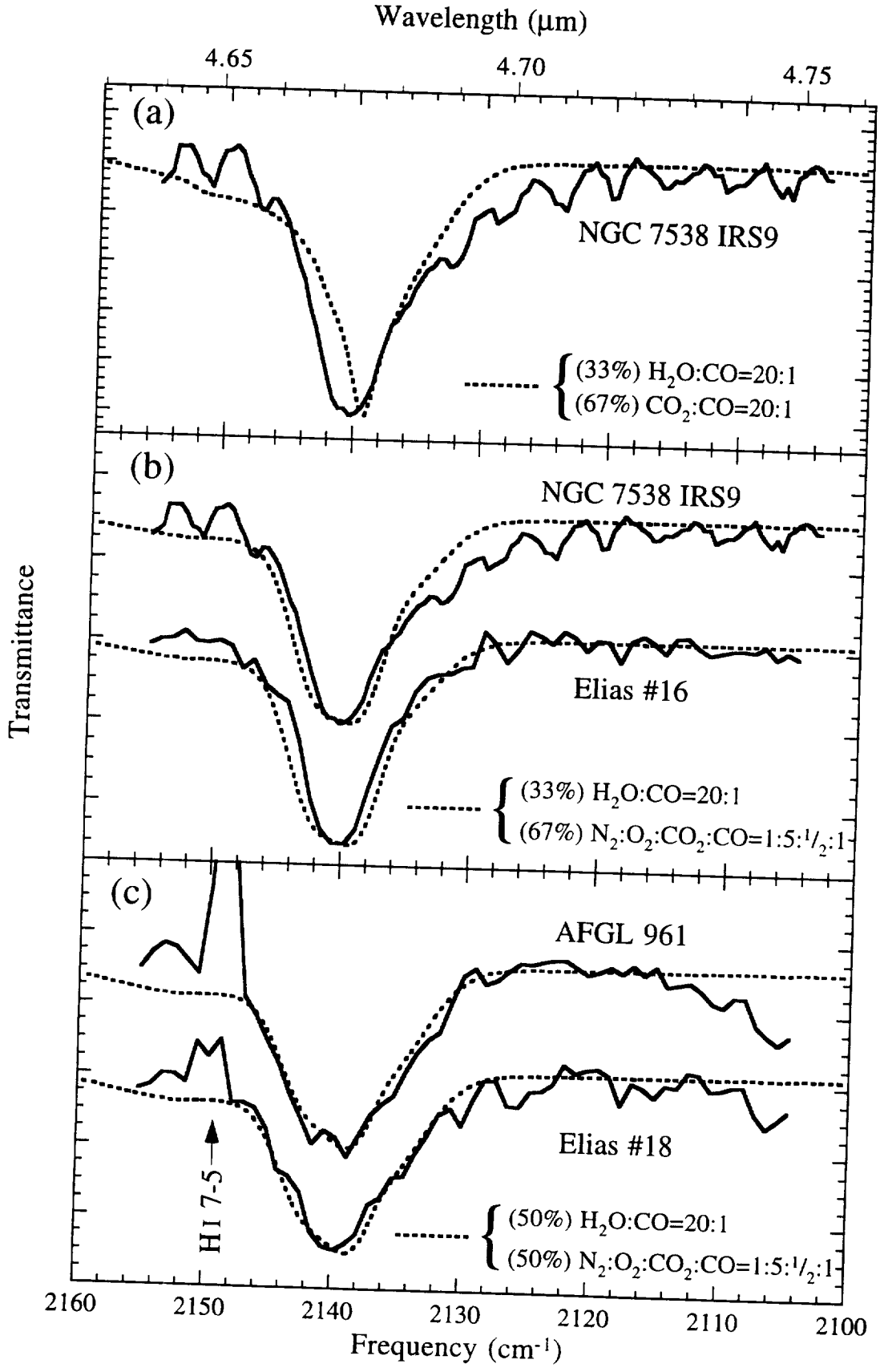
Wavelength (μm)
4.65
4.70
4.75
(a)
NGC 7538 IRS9
(33%) H2O:CO=20:1
(67%) CO2:CO=20:1
(b)
NGC 7538 IRS9
Elias #16
(33%) H2O:CO=20:1
(67%) N2:O2:CO2:CO=1:5:1/2:1
(c)
AFGL 961
Elias #18
H I 7-5
(50%) H2O:CO=20:1
(50%) N2:O2:CO2:CO=1:5:1/2:1
Transmittance
2160
2150
2140
2130
2120
2110
2100
Frequency (cm-1)